

Master Thesis

# Nano-Opto-Electro-Mechanical-Systems for photon control

Nicolas R.H. Pedersen

Advisor: Leonardo Midolo

Submitted: May 31, 2022

This thesis has been submitted to the The Faculty of Science, University of Copenhagen

# Acknowledgments

This work is the result of research conducted in the HY-Q research facility headed by Peter Lodahl. Specifically work was done in the new NANOMEQ subgroup lead by Leonardo Midolo, who has been an amazing supervisor throughout the project and i am deeply thankful for that. A large amount of gratitude needs to be send towards Rodrigo Thomas who spent countless hours with me in the lab and his office discussing, theory and sometimes surprising results that were observed.

A large appreciation also needs to be given to Zhe Liu who fabricated the structures allowing for the experiments carried out throughout this process. Even though a large number of the samples proved to be faulty throughout the process he never backed down and always took the necessary time for SEM-imaging and discussions about fabrication issues.

Finally i will thank my friends and family for supporting me throughout the entire educational process. They have been a constant source of moral support, and has helped me a lot through the harder parts of this work.

# Abstract

Quantum operations, useful towards quantum computing, quantum networks and quantum cryptography requires the ability to manipulate multiple parameters of single photons. In free space this proves to be challenging due to the evasive natures of single photon sources and operations. Quantum photonics serves as a superior alternative, enabling near deterministic on demand single photons along with possibilities of generating a multitude of single photon operations required for quantum computing. These are build from semiconducting single photon sources referred to as quantum dots (QD). Such QD's are embedded in photonic circuits and requires cryogenic temperatures. Furthermore these can be embedded in GaAs structures constituting waveguides enabling the confinement of light. To reach further goals of manipulating single photons for performing advanced quantum protocols, it is a requirement to have switches and quantum gates which are compatible with cryogenic temperatures.

The project investigates the possibility of using Nano-Opto-Electro-Mechanical-Systems as the basis for such operations. These are interesting as they are functional with fast switching times near the coherence times of the single photon sources at hand. Furthermore they gain an advantage over previously demonstrated structures such as thermo-optical phase shifter due to the low voltage requirement rather than heating the structures making them compatible with cryogenic temperatures. This work show both the implementation of a full  $2\pi$  phaseshift imparted by NOEMS structures at low voltages and fast switching speeds, along with the possibility of combining multiple NOEMS devices in the same device with independent control. The settings of the devices are stable as the phase noise has was shown to have a variance of  $\approx 10^{-5}$ . Furthermore the mechanical properties of such structures are studied in greater detail, allowing for even faster switching speeds with resonant driving, which could prove useful towards photon demultiplexing schemes.

Furthermore this project tackles the full Bloch sphere rotation characterisation including both phase shift and switching ranges arising from the case that there will always be some form of fabrication limitation on the symmetrical properties of the constructed devices. Finally a proposition for an NOEMS based architecture enabling the rotation to any arbitrary point on the Bloch sphere is presented. This architecture is build on devices that has been demonstrated independently through experiments. Coupling this with the ability to perform independent actuation of NOEMS structures in the same device this gives promising prospects of realizing any  $2 \times 2$  unitary using NOEMS based devices with single photons generated from quantum dots in the near future.

# Contents

<b>Acknowledgments</b>	<b>i</b>
<b>Abstract</b>	<b>ii</b>
<b>I Overview</b>	<b>1</b>
<b>1 Introduction</b>	<b>2</b>
<b>II Methods and theory</b>	<b>6</b>
<b>2 Theory</b>	<b>7</b>
2.1 Overview . . . . .	7
2.2 Optical NOEMS theory . . . . .	7
Brief waveguide theory . . . . .	7
General NOEMS theory and switching . . . . .	9
NOEMS as phase shifter . . . . .	11
Cascading NOEMS devices . . . . .	14
2.3 simulations . . . . .	14
Simulating the devices . . . . .	14
2.4 Electro-mechanical theory . . . . .	17
Electromechanics of the device . . . . .	17
Pull in instabilities and Dynamics - lumped model . . . . .	19
Resonant driving . . . . .	21
2.5 Chip design and experimental setup . . . . .	22
Chip and device design . . . . .	22
Experimental setup . . . . .	23
Symmetrical phase shifters - chip design . . . . .	24
Devices analyzed . . . . .	24
Experimental Setup and measurement theory . . . . .	25
Optimal waveguide geometry . . . . .	28
Fabricational limitations . . . . .	29
<b>III Experimental results</b>	<b>32</b>
<b>3 Results</b>	<b>33</b>
3.1 Phase shift measurements . . . . .	33
3.2 Switching capabilities . . . . .	37
Full Bloch sphere rotation . . . . .	38
3.3 Symmetrical phase change . . . . .	39

3.4	Full rotation on width optimized devices . . . . .	40
3.5	Full 2x2 operation . . . . .	42
3.6	Mechanical Properties . . . . .	46
3.7	Noise measurements . . . . .	49
3.8	Resonant driving . . . . .	50
3.9	Phase stability . . . . .	53
3.10	MMI response . . . . .	55
<b>IV Discussion and outlook</b>		<b>57</b>
<b>4</b>	<b>Outlook</b>	<b>58</b>
	Phase rotation . . . . .	60
	Future work . . . . .	61
	Future work - mechanical modes . . . . .	61
<b>A</b>	<b>Phase shift measurements</b>	<b>63</b>
	A.1 Optimizing tethers . . . . .	63
	A.2 MMI - theory . . . . .	63
	A.3 Switching speed . . . . .	64
	A.4 Mechanical modes simulations . . . . .	64
<b>Bibliography</b>		<b>66</b>

Part I  
Overview

# Chapter 1

## Introduction

The world of quantum technology based on optics is in rapid development. Recent results show the promising prospects of using electron-hole excitations in semiconductor-based quantum dots as a reliable single photon-source [1]. These can be accurately controlled to generate one photon at a time. This is useful towards building a photonic network sending any N-photon input state to an arbitrary N-photon output state including phase relations. This process corresponds to the ability of performing any NxN Unitary on the input photon state. The building blocks for such networks are 2x2 unitaries which allows for up scaling to any NxN unitary, eg via the architecture shown in figure 1.2.a [2],[3],[4]. These operations would be beneficial towards a wide range of quantum optical technologies such as Boson sampling, quantum cryptography and quantum computing. This method can potentially vastly surpass any current technology made from classical processors [5]. In a path encoding scheme such an operation requires the ability of manipulating single photons in a photonic circuit, this includes manipulating the path which the photon takes through the circuit along with a phase difference between 2 output ports. Concretely these 2 properties can be met by the use of a tunable beamsplitter, capable of switching the light completely between 2 paths, along with a tunable phaseshifter capable of producing a full phase shift of  $2\pi$  on one path with respect to the other.[6]

One method of achieving these goals is via the use of Nano Opto Electro mechanical system (NOEMS) based devices in a photonic circuit. These devices can implement a tunable switch, as a gap variable directional coupler, where the distance between the waveguides in the active part of the system can be altered via electric actuation of the system [7]. This is sufficient for the switching between 2 paths in a photonic circuit, thus one of the 2 required devices can readily be realized. However there is still need for a phase shifter in order to do the full unitary operation. As of now this has mainly been done in photonic circuits via the use of thermo optical phase shifters [8]. Here a temperature change is made in the medium where the light is propagating, thus inducing different optical path lengths leading to a phase shift. These current state of the art thermo optical phase shifters requires a large footprint in the order of  $100\mu\text{m}$  and their switching times are slow compared to those of NOEMS [9], and a key requirement is that the switching speeds are compatible to the coherence times of the quantum dots which typically in the range of  $\mu\text{s}$ [10]. Furthermore the current state of the art Bloch sphere operations can reach a minimum variance of  $\approx 10^{-5}$  when dialing a certain setting [11]. Finally as the thermo-optic phaseshifters requires a change in the temperature they are not compatible with cryogenic temperatures which is a requirement for single photons based on quantum dots [12]. We thus seek a novel NOEMS based solution to the phase shifter, with faster switching times, smaller footprints of the devices and the capability of direct on chip implementation at cryogenic temperatures.

There are a couple of methods in which a phaseshifter can be constructed with the use of NOEMS. One method is using asymmetrical waveguides in the active part of the device, the working principle is thus that the 2 waveguides will have varying optical path properties and thus different propagation constants for the light. When the coupling between the 2 waveguides are changed one arm will pick up a phase with respect to the other arm due to the longer optical path length [13]. These effects has been demonstrated, albeit with results that are far from satisfactory in order to reach a full  $2\pi$  phase shift between the output arms. Another method is to use a system based on a symmetrical relation between the waveguides [7]. This is ensured by the use of a 50/50 beamsplitter in connection with a NOEMS device. Here the optical properties of the system is changed by varying the distance between the symmetrical waveguides, thus by adding one such device on of of the paths in a 2x2 system a phase shift is introduced.

Recent developments in NOEMS based system have shown that such structures are able to act on single-photons at low voltages while still keeping the overall device compact. Previously a switch has been demonstrated at large speeds and a low required voltage, leading to a low power consumption [7]. The question is thus whether such devices are capable of working as a satisfactory phase shifter, while still keeping the advantages over Thermo Optical phase shifters. Another advantage of such a NOEMS based device would be the ability to integrate with single photon sources such as quantum dots in waveguides as they are constructed in a material allowing for direct QD implementation (GaAs) and are highly functional at cryogenic temperatures. [7][12]

The ability to achieve both a tunable splitting ratio, and a phase change with 2 independent NOEMS devices, would fulfill the requirements to do a full 2x2 Unitary operation on single photons. This would correspond to the ability of constructing any single qubit state.  $|\Psi\rangle = \alpha|0\rangle + \beta|1\rangle$ . The visual example of such state is usually represented via the Bloch sphere. Here the single qubit states lie on the surface of the Bloch sphere as they are normalized such that  $\langle\Psi|\Psi\rangle = 1$ , furthermore requiring that  $\alpha^2 + \beta^2 = 1$ . Any general state can thus be described by 2 angles  $\{\theta, \phi\}$  as  $|\Psi\rangle = \cos(\theta/2)|0\rangle + \sin(\theta/2)e^{i\phi}|1\rangle$  up to a global non-observable phase [14]. A schematic of the Bloch sphere and the associated aforementioned rotations is seen in figure 1.1. In a setup with 2 independently NOEMS devices, one for switching and one acting as a phase shifter, these parameters can be understood in terms of how the devices act on the light. The requirements to reach any point on the Bloch sphere is thus a tunable splitting range  $\theta/2 \in [0, \pi]$ , corresponding to the ability of fully switching the light between 2 output ports, the transmitted and reflected, corresponding to  $|0\rangle$  and  $|1\rangle$  respectively. The other parameter needed is the phase difference between the 2 output ports, where the requirement is the ability to do a full  $2\pi$  phase change such that  $\phi \in [0, 2\pi]$ . This architecture is presented in figure 1.2.b

A single unitary and thus a single qubit rotation is not that interesting in and on itself, however it has been demonstrated that the ability to do arbitrary and unitary 2x2 operations are sufficient to make any arbitrary NxN unitary operation. An NxN network requires  $N(N - 1)/2$  unitary 2x2 operations.[2]

The aim of this thesis is thus to construct the necessary building blocks for such operations based on NOEMS systems, with the primary focus being the novel phase shifter capable of doing a full  $2\pi$  rotation, as the possibilities of constructing a tunable beam splitter based on NOEMS structures has already been demonstrated [7]. The possible applications of such a device is not only limited to unitary operations, but are instead suitable for any single photon experiment requiring phase shifting or switching. Further-

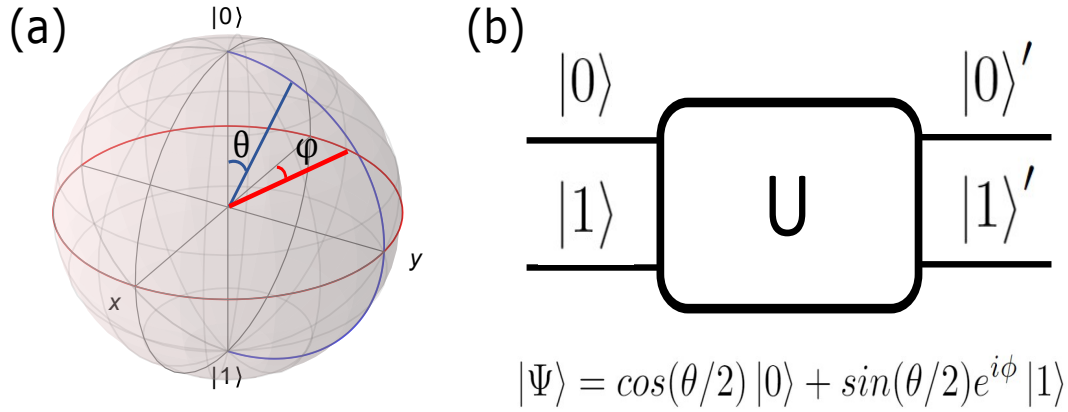


Figure 1.1: **Bloch Sphere with rotations required for Unitary operations** Schematic example of the Bloch sphere with the 2 rotations that are minimally required in order to do any unitary operation on qubits. **(blue)**: Rotation corresponding to the tunable beamsplitter, being capable of switching completely between the 2 output ports, corresponding to a  $\pi$  rotation over the z-axis of the bloch sphere. **(red)**: Rotation corresponding to a phase change between the 2 output ports, a full  $2\pi$  rotation on the x-y plane is required

more the existing switches will be optimized and analyzed in greater depth with regards to the mechanical modes, which are a limiting factor in switching speeds, along with a full characterization of the capabilities of the device along with possible limitations.

The ability to actuate 2 separate NOEMS devices independently in a single circuit is yet to be demonstrated. This is an important step towards the of performing a  $2 \times 2$  unitary and even more so towards further up scaling of the system. Thus the ability to perform such operations with independently actuated devices will also be shown in this work.

Previously a tunable beamsplitter capable of switching light completely from one output waveguide to the other has been demonstrated. This can still be optimized specifically in terms of switching speed which is a key element in upscaling the circuit. Finally resonant driving of the system might be beneficial towards the use in demultiplexing of single photon sources [15]. Thus we seek to improve the switching speeds and capabilities of this part of the circuit.

The main result from this thesis are thus the following:

- Characterization of the devices, including quality factor determinations as a factor of different variables, switching speed capabilities and noise stability measurements. Found in section 3.6-3.9
- The demonstration of a phase shifter based on NOEMS devices capable of producing a full  $2\pi$  - phase shift between 2 output ports based on asymmetrical design of the waveguides. shown in section 3.1.
- Demonstration of actuability of 2 independent NOEMS devices connected in the same circuit showing promising results for the realization of any  $2 \times 2$  unitary based on NOEMS structures. Reported in section 3.5
- Further optimization of existing switches build on NOEMS including switching time and switching capabilities. Described in section 3.4 and 3.8

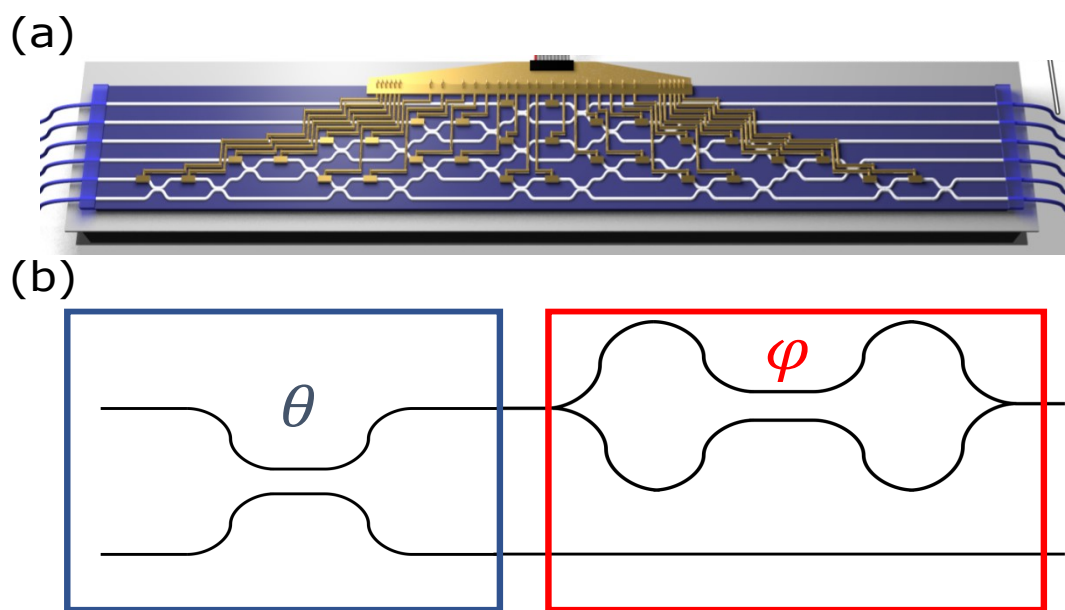


Figure 1.2: **Full network and a sketch of a single 2x2 unitary** (a): Example of a full unitary circuit. From [8]. Here numerous elements can be seen which are all actuated through external controls.(b): The proposed 2x2 unitary which was designed and tested in this project. The first part constitutes the tunable splitting range while the second part is responsible for the phase shift between the 2 output arms.

Part II

Methods and theory

# Chapter 2

## Theory

### 2.1 Overview

As stated in the introduction we search for devices allowing for arbitrary rotations on the Bloch sphere. For this both a tunable switch and a tunable phase shift is needed. Both of these will be constructed via NOEMS devices having different optical and mechanical properties, possibly allowing for the realization of a full 2x2 unitary compatible with the cryogenic temperatures, a strict requirement for the single photon sources (QD's) which are to be used with NOEMS devices.

The following chapter will provide all the theoretic background necessary for the project. This includes the optical waveguide theory which is the principle of NOEMS devices, the electro-mechanical theory which allows for the switching/phase change capabilities, results from simulations and thoughts on the chip design necessary for successful fabrication of devices with the desired abilities.

### 2.2 Optical NOEMS theory

The following section provides the theory needed in order to understand the optical effects which we wish to exploit.

#### Brief waveguide theory

The optical properties of waveguides provides the main working principles of the NOEMS devices with regards to the optical effects. In general waveguides are made from a slab of dielectric material having a larger refractive index compared to the surrounding material, this enables confinement of light within the waveguide [16]. Furthermore it is made thin in one direction, for the purposes of this we chose it to be the z-direction. This forces the incident light to propagate along plane in the x-y direction.

Understanding the fields propagating in the waveguide is of great importance, as it will explain coupling effects which ultimately makes the NOEMS structures interesting. First we consider Maxwell equations in a neutral medium such that  $\rho = 0$  and  $j = 0$ . furthermore the medium has a refractive index  $n(\mathbf{r})$ . The corresponding electrical field which is the solution to the wave equation that can be obtained from Maxwells equation is then [17]

$$\nabla^2 \mathbf{E}(\mathbf{r}, t) - \mu_0 \epsilon_0 n^2(\mathbf{r}) \frac{\partial^2 \mathbf{E}(\mathbf{r}, t)}{\partial t^2} = 0 \quad (2.1)$$

Supposing a radial frequency  $\omega$ , and that the field is given by  $\mathbf{E}(\mathbf{r}, t) = \text{Re}[E(\mathbf{r})e^{i\omega t}]$  the Helmholtz eq for the amplitude  $\mathbf{E}(\mathbf{r})$  is obtained

$$\nabla^2 \mathbf{E}(\mathbf{r}) + k^2 + n^2(\mathbf{r})\mathbf{E}(\mathbf{r}) \quad (2.2)$$

$k$  is here the norm of the wavevector  $\mathbf{k}$  and is given by the dispersion relation  $k = \omega/c$ . When considering a geometry where the wave travels along the  $x$  direction, with  $z$  being the thickness of the waveguide and  $y$  being the width the field can be decomposed to  $\mathbf{E}(\mathbf{r}, t) = \mathbf{E}(y, z)e^{-i\beta x}$  then we can rewrite the equation above as

$$\left(\frac{\partial^2}{\partial y^2} + \frac{\partial^2}{\partial z^2}\right)\mathbf{E}(y, z) + [k^2 n^2(\mathbf{r}) - \beta^2]\mathbf{E}(y, z) \quad (2.3)$$

Finally supposing that  $\partial/\partial z = 0$  the equation can be separated into 2 equations.

$$\frac{\partial^2}{\partial y^2}E(y) + (k^2 n_2^2 - \beta^2)E(y) = 0 \quad |x| > a/2 \quad (2.4)$$

$$\frac{\partial^2}{\partial y^2}E(y) + (k^2 n_1^2 - \beta^2)E(y) = 0 \quad |x| < a/2 \quad (2.5)$$

where the requirement  $|x| < a/2$  is for light within the dielectric material and  $|x| > a/2$  is outside. In the specific case where  $kn_1 > \beta > kn_2$  the amplitude  $E(y)$  is sinusoidal within the waveguide and has an exponential decay outside the waveguide. The light propagates in different modes within the waveguide, usually 2 types of modes are propagating in the waveguide, namely the Transverse Electric (TE) and the Transverse Magnetic (TM) modes. Here however only the TE-modes are studied as the input/output gratings ensure that only these modes can be coupled to the waveguides [18]. A number of TE-modes can propagate within the waveguides, determined by the geometry of the waveguide and the refractive index of the material that is used. This is evident from the fact that there is an endless amount of sinusoidal solutions to the equations above, however the geometry of the waveguide determines which of these solutions actually fulfill the

$$kn_1 > \beta > kn_2$$

as  $\beta$  is geometry dependent. A larger waveguide, with respect to the width and thickness, will support a larger number of modes. We are interested in the regime where only a single TE-mode is propagating in the waveguides, furthermore the waveguides that are used here are GaAs waveguides with a refractive index of  $n_{\text{GaAs}} = 3.48$ . Through previous experiments and COMSOL studies we have concluded that only a single TE-mode is propagating in the region where the GaAs waveguide width is  $> 250$  nm and a thickness of 160 nm, as long as the wavelength in question is  $\approx 930$ nm corresponding to the resonance of current state of the art quantum dots [19]. examples of the lowest order TE-modes for different waveguide widths still in the single mode regime can be seen in fig.2.1.

An important aspect of the modes propagating in the waveguide is that there will be a certain amount of the mode which is located outside the actual waveguide, given by the portion of the field having exponential decay arising when  $|x| > a/2$  from the solution of eq 2.4. This is the evanescent part of the mode which both have useful features but also serves as the main source of loss in the system. Firstly the loss in the system can be explained by this evanescent part of the field, as surface roughness will lead to scattering from this part [20]. Thus a larger evanescent field will lead to larger losses. The evanescent field is however also an important aspect of the systems, as the field located outside the waveguides will leak into nearby situated waveguides which can be used for directional coupling [21]. This is the main working principle of the NOEMS structures, along with the ability to control the distance between the waveguides in the system.

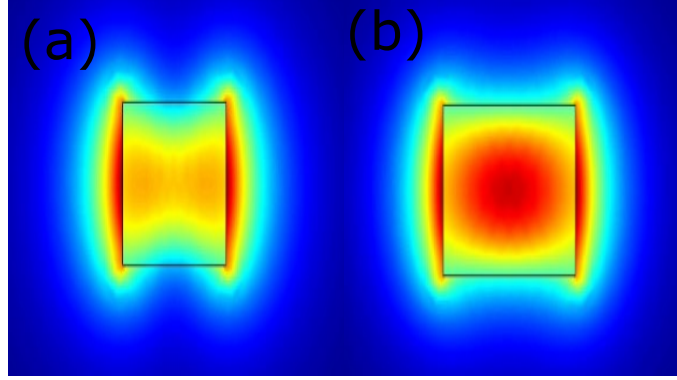


Figure 2.1: **Comsol simulation showing the y-field of the lowest order TE-modes from waveguides with different widths** (a) The lowest order TE-mode of a GaAs waveguide where the thickness is  $t = 160nm$  and a width of  $w = 190nm$  Here a larger part of the mode is evanescent. (b) The lowest order TE-mode of a GaAs waveguide where the thickness is  $t = 160nm$  and a width of  $w = 225nm$  Here a significantly smaller portion of the mode is evanescent

### General NOEMS theory and switching

First and foremost it is important to understand the optical properties of the devices that are designed. The NOEMS devices works on the principle of gap variable directional couplers. Such a system consists of 2 parallel waveguides in close proximity, thus allowing the evanescent fields to leak between the waveguides. The strength of coupling effects between the waveguides can be altered by varying the gap distance between the waveguides, as coupling is determined by the overlap integral between the mode in one waveguide and the evanescent field of a nearby waveguide [22]. Such a process is sketched in figure 2.2. We are working with waveguides preferentially only supporting the lowest order TE-modes (Transverse electric), as we ensure through grating that we only couple to TE-modes, thus mode profile will be proportional to  $\cos(\alpha x)$ . Likewise the evanescent field of the other waveguide is proportional to  $\exp(-\kappa x)$ . Here  $x$  is the position in the direction where there is separation between the waveguides. The constants are  $\alpha = \sqrt{n^2 k^2 - \beta^2}$  with  $k$  being the wavenumber  $k = 2\pi/\lambda_0$  where  $\lambda_0$  is the free space wavelength of the light, and  $\kappa = \sqrt{\beta^2 - 1}$ . This can be evaluated by solving Maxwells equation for the individual waveguides as  $\beta = n_{eff}\kappa$ , where  $n_{eff}$  is the effective refractive index of the mode propagating in the waveguide. this value is dependent on the geometry of the waveguides in use, a simulation of this can be seen in figure 2.4. The coupling strength is thus given as

$$g = g_0 e^{-\kappa d} \quad (2.6)$$

Here  $d$  is then the distance between the waveguide, which can be varied to change the coupling. The other factor  $g_0$  is however constant and solely depends on individual waveguide properties, such as their  $\beta$ , widths and refractive index of the waveguide material. Throughout this project GaAs  $n = 3.48$  was used when making the waveguides

When working with the 2 parallel waveguide system it is convenient to describe it in a diagonalized basis. diagonalization is done by starting from a matrix of the system in a basis of the 2 output ports. Here the matrix describing the NOEMS system is given as

$$\begin{pmatrix} a_{1out} \\ a_{2out} \end{pmatrix} = \begin{pmatrix} \beta_1 & g \\ g & \beta_2 \end{pmatrix} \begin{pmatrix} a_{1in} \\ a_{2in} \end{pmatrix} \quad (2.7)$$

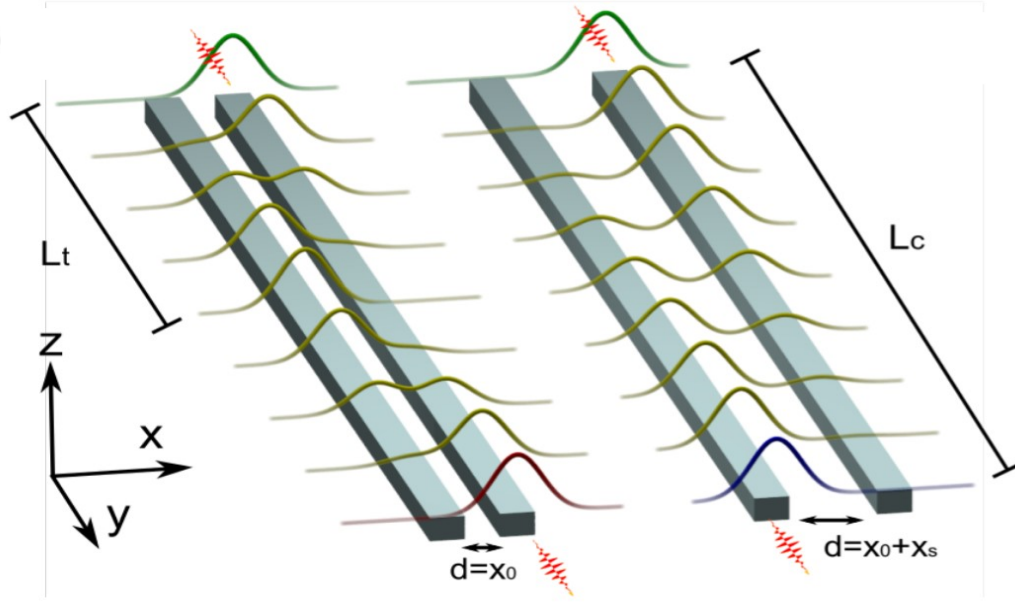


Figure 2.2: **Operation principle of the NOEMS device** The working principle of the NOEMS devices as a switch. Light is inserted into one of the waveguides, and the resulting mode profile is shown. In the initial setting where  $d = x_0$  the coupling is maximal as there is a large overlap integral between the mode and the nearby waveguide. As gap between the waveguides is increased to  $d = x_0 + x_s$  the coupling is decreased leading to a different output in the 2 ports. This shows the example of full switching between the output ports.

Where for a completely symmetrical setup  $\beta_1 = \beta_2$ . Here  $a_1$  and  $a_2$  corresponds to the 2 waveguides, where the  $a_{i\text{in}}$  denotes the point of injection and  $a_{i\text{out}}$  denotes the point where the light is recollected at the end of the system. Equation 2.7 can be diagonalized by introducing the normal modes  $a_s = (a_1 + a_2)/2$  and  $a_{as} = (a_1 - a_2)/2$  which are called the symmetric and anti-symmetric modes respectively [23]. When injecting light through either  $a_1$  or  $a_2$  both modes are excited and will propagate given their propagation constants.

$$a_{1,2} = \frac{1}{2}(a_s e^{-\beta_s} \pm a_{AS} e^{-\beta_{AS}}) \quad (2.8)$$

Where  $\beta_s$  and  $\beta_{AS}$  are the propagation constants for each of the symmetric/anti-symmetric mode. For identical waveguides the intensity in the 2 output ports are then given by  $I_1 = |a_1|^2$  and  $I_2 = |a_2|^2$  as

$$I_1 = I_0 \sin^2\left(\frac{\beta_s - \beta_{AS}}{2}\right) = I_0 \sin^2(gy) \quad (2.9)$$

$$I_2 = I_0 \cos^2\left(\frac{\beta_s - \beta_{AS}}{2}\right) = I_0 \cos^2(gy) \quad (2.10)$$

Here  $I_0$  is the initial intensity in the system,  $y$  is the length of the coupled section of the 2 waveguides, and  $g = (\beta_s - \beta_{AS})/2$ . This enables the definition of the transfer length, which is the propagation length required to switch the light completely from one waveguide to the other  $L_t = \frac{\pi}{2g}$ . Thus we can define the output intensity of transmission port one as

$$I_1 = I_0 \sin^2\left(\frac{\pi}{2L_t} y\right) \quad (2.11)$$

The working principle of switching mechanisms in the design is thus to vary  $L_t$  while keeping the active device length  $L_c$  constant, meaning the value of  $y$  at the output port is

kept fixed from the fabrication of the device. As  $L_t$  is varied when varying the coupling strength  $g$ , this value can be changed by actuating the device thus varying the distance between the waveguides. Previously devices with full 100/0 to 0/100 switching has been shown, in terms of the Bloch sphere rotation this corresponds to a  $\pi$  change in  $\theta$  [7]. In the following project the coupling length of the devices is however increased by cascading multiple NOEMS devices as explained on page 14. We thus expect to see larger effects, even on the order of  $\theta > 2\pi$ .

### NOEMS as phase shifter

The aforementioned theory described the usability of NOEMS devices as a switching device. However there are numerous assumptions made in order to only enable switching without other optical effects. One such is that the waveguides are completely symmetrical. In reality different kinds of fabrication limitations give rise to asymmetries in the geometries of the parallel waveguides, furthermore asymmetric effects might even be created on purpose in order to obtain phase shifting effects from the system [24]. Previously the assumption of identical waveguides leading to  $\beta_1 = \beta_2$  was made. However if the waveguides are asymmetrical, either on purpose, or through errors in the fabrication process, this statement is no longer valid. The resulting effect will be that the  $\beta_i$  values constituting the propagation speed of light in the respective waveguides will be varying. The amount of variation in the effective mode index  $n_{eff} \propto \beta$ , as a function of waveguide widths at a fixed thickness can be seen in figure 2.3.

This will still give switching capabilities as the changes are not large, thus the previously mentioned theory is approximately true (It mainly limits the amount of extinction between the 2 ports as we are no longer able to go from 100/0). However when changing the gap, and the coupling strength, we are also changing the optical path length which the photons undergo before exiting at each of the output ports. This will lead to a different phase experienced for photons exiting at output 1 compared to output 2. Considering a system producing a 50/50 splitting ratio and comparing the path length to a case where the system is completely decoupled giving a 100/0 splitting ratio it is evident that the phase at the different output ports will be different if the  $\beta$ 's of the 2 waveguides are no longer identical. Thus a system composed of 2 asymmetrical waveguides will both constitute a  $\theta$  and a  $\phi$  shift when considering the imparted rotation on the Bloch sphere. As the changes to the effective refractive index are small and due to the experiments that was carried out in the "short" NOEMS based tunable switches these effects has not been seen. However as we greatly increase  $L_c$ , the phase that is picked up will vastly increase as the effect scales linearly with  $L_C$ . This is one of the reasons that we chose to cascade the NOEMS device as a full  $2\pi$  shift in  $\phi$  is of great interest. Noteworthy is however that while such a device is likely to produce the full  $\theta$  and  $\phi$  rotations on the Bloch sphere simultaneously, the rotations are not independent. A single device of this type will thus not be sufficient to reach any arbitrary point on the Bloch sphere. This means that another device will still be needed, as it would in an architecture with 2 independent Bloch sphere rotations. However if the full phase shift is obtainable the only remaining requirement is a symmetrical NOEMS system capable of doing the necessary rotation in  $\theta$ , without applying a substantial phase shift rotation in  $\phi$ .

A final remark on the properties of the asymmetrically designed NOEMS system is that while increasing the amount of symmetry - thus the  $\Delta n_{eff}$  between the waveguides - should seemingly lead to a larger phase shift at the output ports, this is only partially the case. For vastly varying differences in the geometry of the waveguides the mode matching requirement, which provides the ability of coupling, will be changed. It is evident from

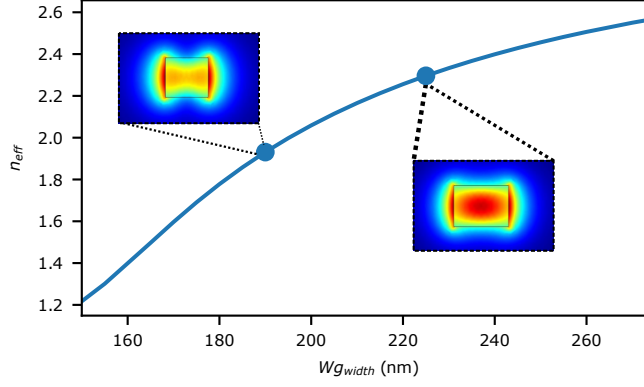


Figure 2.3: **Effective refractive index  $n_{eff}$  as a function of waveguide widths** Comsol simulation based on a 180 nm thick waveguide with varying widths, finding the excited modes in the waveguide. In this region only a single mode is propagating, however with different  $n_{eff}$  Furthermore the gradient  $\Delta n_{eff}$  varies over the wavelength, suggesting a larger amount of loss due to surface roughness for narrow waveguides. The insert show the lowest order TE-modes for the waveguide at different wavelengths, 190 nm and 225 nm respectively.

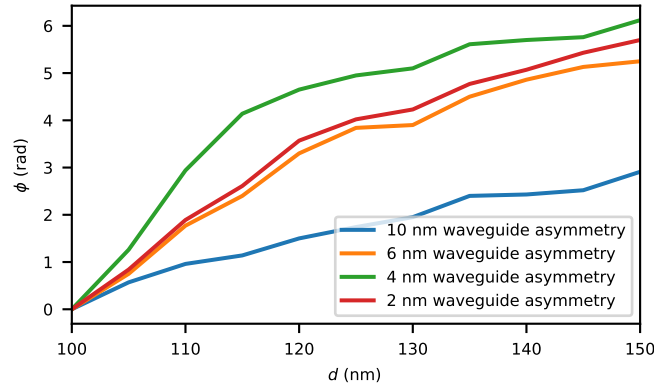


Figure 2.4: **Obtained phase rotation  $\phi$  in an asymmetric geometry with varying levels of asymmetry** It is evident that there is a "sweet" spot in the level of asymmetry when considering the resulting phase shift. A low asymmetry has a small difference in the  $\beta_i$  values for the different waveguides, whereas a large asymmetry does not allow for sufficiently large couplings between the waveguides. The optimal asymmetry is likely dependent on the actual widths of the waveguides, as a wider waveguide will require a larger asymmetry to obtain the same amount of change in  $\beta_i$  between waveguides

figure 2.1 that the mode profiles of the resulting modes given 2 vastly different waveguide widths are differing a lot. This will lead to a lower coupling by having a smaller overlap integral, thus limiting how much we can change the path of the light, a necessity for obtaining the phase shifting effects of the device. This will be studied in detail through COMSOL studies in order to find the right balance between the amount of asymmetry in the waveguides and the phase shifting effects. In order to do this the same simulation, with different levels of asymmetry in the setup was carried out and the result is seen in figure 2.4. Here the simulations revolves around a waveguide with at a width of 200 nm, whereas the other waveguide has the amount of asymmetry added.

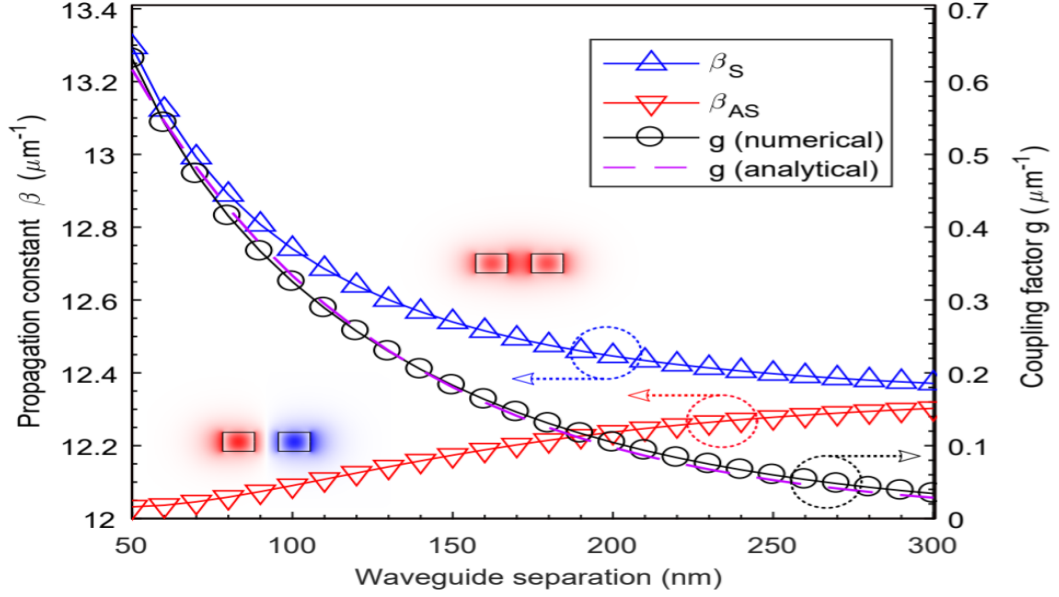


Figure 2.5: **Varying  $\beta$  and  $g$  factors as a function of the distance between the waveguides** Varying the gap size between the parallel waveguides will change the different factors in the diagonalized basis. Here it is evident that there is a large variation in the  $\beta_S$  with varying gap sizes between the waveguides. This allows the NOEMS device to be used as a phase shifter if it is applied to one arm of a 2 mode circuit.

Designing the device to have asymmetrical waveguides is however not the only way to obtain a phase shift via NOEMS devices. From equation 2.4 it is evident that there is a sign difference in the asymmetrical part of the mode when considering which of the input ports  $a_{1,2}$  is pumped. Evidently if light is inserted exactly with a 50/50 ratio of intensity in  $a_1$  and  $a_2$  simultaneously the corresponding propagating mode will only be the symmetrical, as the asymmetric contribution from both ports will cancel out. This can be utilized in order to obtain a tunable phase shifter. By considering 2 completely parallel waveguides, a 50/50 MMI (Multi-Mode interferometer) going from a single waveguide to 2 waveguides can be used on one of these initial paths, the MMI effect is explained in Appendix A.2. These 2 new waveguides constitute a NOEMS, where only the symmetrical mode will be pumped, as the initial intensity is divided evenly between the waveguides. Such an architecture of this setup is shown schematically in figure 1.2.b in the red box. Now the  $\beta_S$  is dependent on the distance between the waveguides, as can be seen from the blue line in figure 2.5, thus if the gap  $d$  is changed we are consequently changing  $\beta_S$  and thus the optical path length. As the other arm is simply a straight waveguide, this will lead to a change in the resulting phase difference at the 2 output ports. If the phase change is sufficient, meaning that  $\phi$  can be tuned to larger than  $2\pi$ , a setup on the type of figure 1.2 will be capable of performing any  $2 \times 2$  unitary. Yet again as the effects on the change in  $\beta_S$  varies slowly while changing  $d$  we require a longer  $L_c$  in order to obtain the desired effects. Furthermore it is not trivial to anticipate how large the effects of a possible non 50/50 MMI operation, or the inevitable asymmetries in the waveguide widths will be in terms of the symmetrically based phase shifter.

## Cascading NOEMS devices

As mentioned in the previous section we need a way to extend the  $L_c$  of the devices in order to obtain the desired phase shifting effects. There are however numerous concerns regarding the design of these new structures. First and foremost the devices are composed of suspended waveguides, this gives limitations on the distance between supporting tethers that are needed to prevent the collapse of the structures. Usually this length is  $\approx 10\mu m$ . In the previously designed structure one such tether was situated in the center of the NOEMS devices to keep the structure suspended [7]. If we desire to extend the length additional tethers are needed leading to a larger amount of inactive device. This is due to the fact that tethers fixes the device in place at the tethering position, thus this part is not gap variable and does not contribute to changes in the coupling  $g$ . This does however turn out to not only be a limitation but also an advantage. The switching speeds of the device is primarily limited to the resonance frequency of the waveguides lowest order resonant mechanical mode. This mode is determined by the geometry of the design, mainly the stiffness of the waveguides, determined by waveguide lengths and widths. Thus when we increase the  $L_c$  of the device this should lower the switching speed compared to previously designed NOEMS devices. However by adding more tethers as required the stiffness of the device is increased, and the mechanical frequencies should depend on the individual cascaded sections and not the entire device itself as we hypothesize that points of tethering acts as fixed points. Thus the only immediate drawback happening from cascading the device is a larger footprint of the device on the chip. This is however necessary if phase shifts on the order of  $2\pi$  are to be obtained, either through symmetry or asymmetry in the device. The total length should however still be shorter than the current state of the art thermal phase shifters.

The exact geometry of the waveguides constituting the NOEMS device will be determined through COMSOL simulations. There are however a couple of noteworthy thoughts which needs to go into the design. First and foremost there is a trade off between the switching speed and the maximal phase shift/switching. A maximal switching speed could be obtained by only having short sections of parallel waveguides between tethers. This would however give a larger part of the device that cant be actuated, leading to an overall longer footprint.

## 2.3 simulations

This section deals with the simulation of the devices which was used in the design process. All simulations were carried out using the Finite element method program COMSOL.

### Simulating the devices

Making such complicated opto-electromechanical structures are not a task that can simply be carried out blindly. Furthermore developing new devices analytically are also not effective. Luckily, Finite elements method based programs allows for the simulations of both the optical and mechanical response of these structures.

The basis of finite element based simulation programs is to not solve the entire geometry at once but in turn subdivide the problem into a number of elements by construction of a mesh over the object in question. These finite elements are then solved with boundary conditions that gives a system of algebraic equations that can be solved. This is afterwards turned in to an approximate solution for the entire domain. The actual real world solution would require a mesh of infinite precision, however this is not feasible due to computa-

tional limitations. Instead it is necessary to determine the mesh size for the given problem, which approximates the actual solution to a desirable degree. In order to do this a mesh convergence is conducted. Here different mesh sizes are tested in order to find the limit where the solution converges to a constant value, determining that this is close to the real world solution on the same problem.

Another important aspect for the simulations in questions is the boundaries around the object. The object will be suspended in air thus having a boundary around it, and it is assumed that no light is reflected back once it has left the devices, either through scattering or other effects. When doing boundary mode analysis, all light incident at the boundaries of interest will be terminated. However these are only placed in the regions where light from the device itself should emerge. Thus for other regions scattering might occur, where light completely escapes the system, never to return. This is solved by adding perfectly matched layers (PML). These act as an artificial absorbing layer, ensuring that no back scattering into the domain occurs in these regions. This acts as if the light field at these points simply escape to infinity rather than getting reflected back into the domain. This is explained in greater depth with the inclusion of such a study in Appendix 1.

When this is ensured for all the different types of simulations these can now be carried out for numerous different parameters in order to obtain a geometry producing the desired responses. As the simulations are complex, it is a demanding task computationally. However symmetries in the geometry can be exploited as to limit the simulated domain, lowering the computational demands drastically. By imposing different boundary conditions on the domain different kinds of symmetries and asymmetries can be created, allowing to only simulate parts of the full domain while still obtaining the full result. Firstly, considering that the length of the object goes in the y direction, the width of the object is in the x direction and that the height of the object is in the z-direction, it is evident that there is a symmetry along the z axis for the domain that we are interested in simulating as there is up-down symmetry in all the structures of concern. Thus the boundary condition of a perfect electrical conductor can be placed on the boundary cutting through the upper half of the object. This leaves us with only half the domain for the simulations. Furthermore for the symmetrical devices there is an additional symmetry in the x axis through the middle of the gap between the waveguides. This is however only for the device in which both of the input waveguides are pumped via the 50/50 MMI, as the tunable beamsplitters will only be pumped from one port at a time to investigate the effects thus breaking the aforementioned symmetry. Here another kind of symmetry is used however, namely the perfect magnetic conductor, which ensures that the simulation is covering the case where only the symmetric mode of the total system is pumped.

For the other devices, such as the symmetrical beamsplitter, which is based on symmetric waveguides, but where only 1 of the inputs are pumped at any given time, only the z-axis symmetry can be utilized, as there is an asymmetry in the pumping of the waveguides. Obviously a similar approach is needed when studying the asymmetric case, where there is a difference between the 2 waveguides in the directional coupler.

Different kinds of simulations are carried out, one with the intend of studying the optical properties of the system with variable gaps between the waveguides. Varying geometries are tested at this stage, including varying widths, coupling lengths and initial separations  $d_0$  one such can be seen in figure 2.6. Another study is used to determine the amount of movement in the waveguides, this is done with a mechanical study of the system where a voltage is applied in order to observe the  $d(V) = x_0 + x(V)$ . For the optical simulation the "Electromagnetic waves, frequency domain (emw)" build in study in

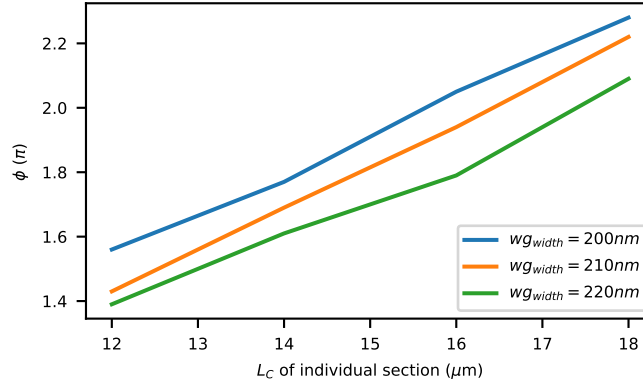


Figure 2.6: **Simulated phase change for a symmetric based phase shifter** COMSOL simulation of the symmetrically based phase shifter. Here it is evident that a  $w_{gwidth} = 210\text{nm}$ , combined with a individual cascading length of  $L_{Cind} = 16\mu\text{m}$  is sufficient to produce a full  $2\pi$ -phase shift.

COMSOL is used. Here the boundary mode analysis is applied to 4 ports, corresponding to the 2 input and 2 output ports. Port 1 is pumped at the desired frequency, and all the optical material constants are applied to the system. It is assumed that movement of the waveguides are constant throughout the entire directional coupler when actuating, this is an approximation as the actual movement will depend on the exact position along the waveguides, especially in the region where tethers are located. It has however been demonstrated previously that this assumption is valid enough to obtain useful results from the simulation [7]. Furthermore another simplification is used, as the device is cascaded with identical copies, only the effects in one of these copies is studied. The assumption is that cascading the device will give exactly same results for each of the individual devices, such that the results obtained can simply be scaled linearly by the number of cascations. This is true as long as the cascaded devices are actually approximately similar to each other. From this, the number of devices needed in succession can be estimated. Finally a study is done on the time dependent behavior of the actuation. This will show the different mechanical modes in the system, we are coupling to these when the actuation signal is done fast and will be the ultimate limiting factor on the speed of the devices. Here it is noteworthy that many mechanical modes will show for the system, however only the optically active modes are of interest. In general modes that changes the gap between the waveguides at different positions along the x-axis of the waveguides. Thus resonances which are only moving the waveguides along the z-direction will be disregarded as these will have little to no effect on the optical properties of the system.

For the mechanical simulations the "electromechanics (emi)" module in COMSOL is used. Here the stationary study is used, as we are mainly interested in the amount of movement induced by the actuators. Only one waveguide, and its associated actuation is studied here, as the amount of movement will be the similar on the other waveguide, even in the case of asymmetries where movement might only vary slightly. Again only one of the cascaded devices are analyzed, as we suppose that these be move independently. For future works more simulations, in larger detail, of the fully coupled cascaded device might be of great interest. Examples of COMSOL structures studied can be seen in Appendix A.4.

## 2.4 Electro-mechanical theory

The following section deals with the theory behind electronic actuation of the system. This process makes for all changes to the optical properties by gap variations via an electronic force.

### Electromechanics of the device

As we are interested in displacing the waveguides in the directional coupler in order to reconfigure the settings by changing the coupling we are using an capacitive nanomechanical actuators. When a voltage is applied the capacitors charge closing the gap on the actuator side and separating the optical waveguides. The capacitance of this structure can be approximated as [7]

$$C(x) = C_m(x) + C_s(x) \quad (2.12)$$

Where  $C_m$  is the capacitance of the metal lines, and  $C_s$  is that of the underlying semiconductor. The waveguides are moved via a shuttle made of a semiconductor beams which is connected to the waveguides in the directional coupler via tethers. The force acting on the shuttle is given by  $F = \frac{1}{2}V^2\frac{\delta C}{\delta x}$ . This structure is however far to complicated for an analytical evaluation, thus a full 3D simulation is needed to estimate the forces. However, it is useful to consider a simpler model to estimate the parameters needed when designing the structure, in order to simulate the parameters within this region. A similar approach was used in [7], and the values found here are being reused for the designs of the structures analyzed in this report. The basis of this simpler analysis is to simplify the system as a parallel plate capacitor model. The force exerted is then approximated to

$$F \approx \frac{1}{2}V^2\epsilon_0L_s \left( \frac{t}{(b_0 - x)^2} + \frac{t_m}{(b_m - x)^2} \right) \quad (2.13)$$

Here the parameters used are  $t_m$  for the thickness of the metal electrode,  $b_0$  is the distance between the actuators at rest,  $L_s$  is the length of the shuttle part, and  $b_m$  is the distance between the metal lines at rest. As in previous works  $t_m = 70nm$  and  $b_m = 500nm$  is used, which is determined by constraints in the fabrication process.  $b_0$  is chosen by taking the pull-in instabilities of the system into account. This constrains to a movement of  $\approx 1/3b_0$ , thus when desiring displacement in the order of  $50 - 100nm$  we chose  $b_0 = 300nm$ . By using Hookes law an expression for the displacement can be obtained.

$$(b_0 - x)^2x - \frac{V\epsilon_0L_s t}{2k_T} = 0 \quad (2.14)$$

Furthermore the elastic constant of the system can be estimated, by neglecting the metal electrodes, which are thin compared to the rest of the system, as

$$k_T = k_{wg} + k_s = 384E \left( \frac{I_{wg}}{L_{wg}^3} + \frac{I_s}{L_s^3} \right) \quad (2.15)$$

Here  $E$  is the Youngs Modulus of the GaAs constituting the waveguides,  $I_{wg}$  and  $I_s$  is the moment of inertia of the waveguide and shuttle respectively and finally  $L_{wg} = L_c + L_{taper}$  is the total length of the waveguide, including the taper in the central region, where the waveguide is connected to the shuttle via a tether. Importantly  $k_T$  is what ultimately restricts the speed at which the device can be reconfigured, as this will give the mechanical resonance frequencies in the system. By reconfiguring the settings faster than the lowest order mechanical frequencies in the system, oscillations are introduced, which will lead to an oscillating coupling factor  $g$ . From the expression of  $k_T$  it

can readily be observed that increasing the total length of the device, will lead to a less stiff device, thus a lower mechanical resonance frequency. On the other hand increasing the length will increase the coupling region, thus requiring smaller displacements to obtain similar results. A method in which to do both simultaneously is by cascading NOEMS structures, in order to maintain the stiffness of the shorter devices while having a larger  $L_C$

An interesting feature is that the resonance frequencies of the waveguides are tuned by actuating the system. This is due to frequency softening, which is voltage dependent [25]. A simple theory for this gives the change in resonance frequency as

$$f^2 = f_0^2 - \frac{\epsilon_0 A_{ele} V^2}{4\pi^2 (g_e - x)^3 m} \quad (2.16)$$

Where  $A_{ele}$  is related to the size of the waveguides,  $m$  being the mass,  $x$  the displacement and  $g_e$  the gap between the resonator and electrode. When the displacement is small, this will give an approximately linear dependence between the resonance frequency squared and  $V^2$ . Furthermore this will only be applicable to the lowest order modes of the waveguides, it does however suggest that the operating speeds at large voltages are somewhat slower than at low voltages.

This effect might prove to be valuable if we want to utilize resonant driving of the system. Here it might be possible to use the resonant frequencies in order to obtain fast switching times. Such a setup can be used for demultiplexing [7][15], here it is however necessary that the different devices in the setup has the same resonant frequencies. This will require that the waveguides are exactly identical, which is not likely due to fabrication errors. It could however be possible to set a DC voltage on top of the resonant driving in order to change the resonance frequencies. It is thus of interest to analyze the range wherein these resonances can be tuned, in order to evaluate whether it is possible to tune 2 separate devices into resonance or not.

Another important aspect of the electromechanical properties of the devices are the phase stability. This is a measure of how well the device can be reconfigured to a given setting and stay there. A certain phase stability is needed in order to realize a useful device for scaling to NxN unitary operation. This is of course dependent on the actual size of the system, as larger system will require larger precision in order to achieve sufficient fidelities. The fidelity is a measure of how well a given intended unitary operation can be reproduced by the system. This can be quantified as [2]

$$F(U, U_s) = \frac{1}{N^2} |Tr(U^\dagger U_t)|^2 \quad (2.17)$$

Here  $U_t$  is the target transfer matrix,  $U$  is the experimentally realized matrix and finally  $N$  is the size of the NxN matrix in question.

The experimentally achievable matrix will depend on numerous different limitations in the setup, including losses and importantly for this part the phase noise. This noise  $\delta\phi$  and  $\delta\theta$  will be a measure of the uncertainty on the set values  $\theta_e$  and  $\phi_e$ , where the  $e$  denotes that these are expected values. The actual phases set will thus be  $\theta = \theta_e + \delta\theta$  and  $\phi = \phi_e + \delta\phi$ . Here importantly the  $\delta$  values can go in either direction with an unknown magnitude, thus limiting the actual settings.

A way to quantify the precision with regards to the size of the circuit is the n-bit precision [26]. When considering an arbitrary Unitary matrix with size NxN, we can denote all the phases needed as

$$\phi_j = \phi_{j0} + \delta\phi_j \quad (2.18)$$

again with the same arguments for the 2 values constituting the actual phase shift, and noting that ( $j=1\dots N^2-1$ ). the phase shift provides an n bit precision when  $\delta\phi_j \leq 2\pi/2^{n+1}$ . It has been demonstrated that a  $n = 10$  bit precision is sufficient for the approximation of a N channel unitary matrix up to  $N \approx 100$ . this precision corresponds to a phase error  $\delta\phi_j \leq 3 \cdot 10^{-3} rad$

The phase noise level in NOEMS structures will primarily be due to unwanted oscillations of the individual waveguides which changes the coupling. It goes without saying that this first and foremost concludes that the operating speeds should be such that oscillations are excited in the structures. When working in this regime we are however not completely free of oscillations. Such oscillations occurs due to different effects, but the largest contributor is due to thermal noise. We hypothesize that thermal effects will be lowered when working in a single photon regime at cryogenic temperatures. We will however do experiments at room temperature, nevertheless we should still get an indication on the maximal phase error in the system.

### Pull in instabilities and Dynamics - lumped model

A simplified lumped element model can be used to describe the mechanical motion and effects when actuating the devices. The system can be modelled as a voltage controlled parallel plate electrostatic actuator [27].

The system will have an important behavior, the so called pull-in voltage. This is explained by the opposite forces of the voltage pulling the plates in one direction and the spring force pulling towards the other. The analysis of the pull-in consists of a stability analysis of the system. Here the system is perturbed from the equilibrium position and it is analyzed if the net force returns the system to the equilibrium position. The force on the upper capacitor plate at a given voltage V and gap g is given by:

$$F_{net} = \frac{-\epsilon AV^2}{2g^2} + k(g_0 - g) \quad (2.19)$$

Here the signs are set such that the positive force increases the gap, and vice versa.  $g_0$  is the gap at rest. When the system is at equilibrium position it will of course imply that the net force is 0. Now examining how the net force varies with a small perturbation  $g_0 + \delta g$  such that

$$\delta F_{net} = \left. \frac{\partial F_{net}}{\partial g} \right|_V \delta g \quad (2.20)$$

Now importantly if the change in net force is positive for the given  $\delta g$  this is an unstable point of equilibrium as the  $\delta g$  is increased further, making the force increase further. On the other hand if  $\delta F_{net}$  is negative then the equilibrium point is stable. Evaluating the force to find

$$\delta F_{net} = \left( \frac{\epsilon AV^2}{g^3} - k \right) \delta g \quad (2.21)$$

Thus for g to be a stable point the parenthesis must be a negative value, implying the condition that

$$k > \frac{\epsilon AV^2}{g^3} \quad (2.22)$$

The equilibrium gap decreases when the voltage is increased, this implies that there is a certain voltage where there is no stability at the equilibrium position. This is regarded as the pull in voltage  $V_{PI}$ . From this we can find the pull in position  $g_{PI}$ , to find this 2 requirements has to be fulfilled, that  $F_{net} = 0$  and that

$$k = \frac{\epsilon AV_{PI}^2}{g_{PI}^3} \quad (2.23)$$

From the above equations we can see that the pull in occurs at

$$g_{PI} = \frac{2}{3}g_0 \quad (2.24)$$

This provides us useful information on the initial gap  $g_0$  as we will need to move the waveguides a certain distance in order to observe the desired effects. From this knowledge we will chose  $g_0 \approx 300nm$ . Furthermore the pull in voltage can be approximated, thereby giving us information on how hard we can drive the system

$$V_{PI} = \sqrt{\frac{8kg_0^3}{27\epsilon A}} \quad (2.25)$$

The above information only deals with stable forces applied to the system and looking at the equilibrium positions when applying different static voltages. The system still consists of a 2 port capacitor system, with one port connected to the mechanical domain and the other to the electrical domain. To describe the system the KVL (Kirchoff Voltage laws) equations are applied to the system, and are manipulated into state form. It is necessary to work with the full set of nonlinear equations as the system is nonlinear. Furthermore when dealing with the dynamics of the system additional parameters needs to be taken into account, this includes the inertia of the plate being moved, a source resistor for the voltage source driving the system and finally mechanical damping forces that arises from the medium surrounding the system. All of this information gives the nonlinear equation, first of the equation for the electrical domain.

$$\dot{Q} = I = \frac{1}{R}(V_{in} - \frac{Qg}{\epsilon A}) \quad (2.26)$$

The equation for the mechanical domain is given by

$$F = \frac{Q^2}{2\epsilon A} \quad (2.27)$$

From these equations we can obtain

$$\frac{Q^2}{2\epsilon A} + b\dot{g} + m\ddot{g} + k(g - g_0) = 0 \quad (2.28)$$

We want to bring the equations into state form, thus 3 state variables should be identified, here we select the following 3 variables.

$$x_1 = Q \quad (2.29)$$

$$x_2 = g \quad (2.30)$$

$$x_3 = \dot{g} \quad (2.31)$$

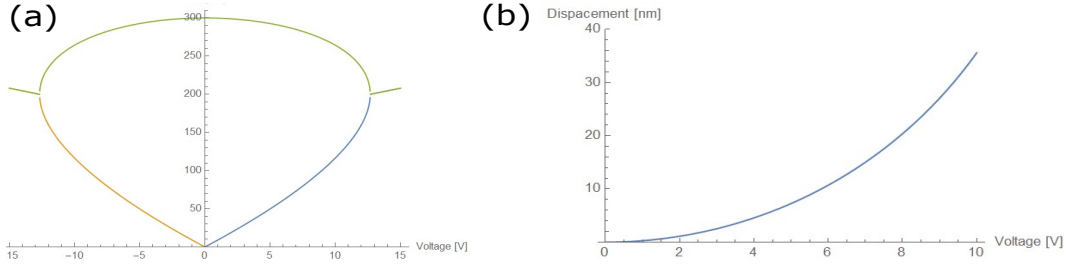


Figure 2.7: **Estimation of pull in voltages and approximate waveguide displacement** (a) showing the stable solutions for the voltage setting (green) and the unstable solutions (orange and blue). The pull in voltage is estimated to be 12V. (b) Estimation of the displacement at a given voltage, this is useful towards simulations.

which gives the following state equations

$$\dot{x}_1 = \frac{1}{R}(V_{in} - \frac{x_1 x_2}{\epsilon A}) \quad (2.32)$$

$$\dot{x}_2 = x_3 \quad (2.33)$$

$$\dot{x}_3 = -\frac{1}{m}(\frac{x_1^2}{2\epsilon A} + k(x_2 - g_0) + bx_3) \quad (2.34)$$

Here it should be noted that  $x_1$  is the charge on the capacitor,  $x_2$  is the gap between the capacitor plates and  $x_3$  is the velocity of the moving plate.  $A$  is the area of the plate,  $R$  is the resistance of the time dependent voltage  $V_{in}$ , and  $\epsilon$  is the permittivity of the surrounding environment (air, vacuum etc.). This allows for the estimating of a static solution giving an estimation on the amount of movement induced at different voltages, furthermore at which voltage levels the solution is stable. Here it is found that we from this crude model expects displacements of  $\approx 50\text{nm}$ , and we should be able to drive the system with up to 12V before reaching the pull in. Aforementioned effects are shown in figure 2.7. Estimations of the amount movement is valuable when simulating the devices to know which optical effects we can anticipate.

## Resonant driving

Until this point it has been described that the resonant modes are preferred not to be excited, and thus in most experiments we are driving the voltage slower than the NOEMS resonance frequencies. This is to ensure that we can actually park the system at a given setting, while not waiting for dampenings of oscillations. Waiting would decrease the switching speed drastically compared to lower than resonant driving. However it is theoretically possible to acquire much faster switching at lower voltages if we were to drive the system resonantly. Resonant driving can be obtained by driving the actuators with a sinusoidal sine wave on the form  $V_{in} = V_0 \sin(\pi \nu_{mn} t / 2)$ , as the force is responding with the square of the voltage applied this will be proportional to  $\sin(\pi \nu_{mn} t)$ . Here  $\nu_{mn}$  is the  $n$ 'th resonant mode of the system. Thus we need to drive at half the frequency of the resonant mode that we are driving. Previously resonant driving of the lowest order modes has been demonstrated [7]. Here it was furthermore seen that for this kind of device there is a difference between the resonant frequencies of the 2 waveguides, even when they are designed to be identical, meaning that the waveguide widths differs by some amount. This effect primarily happens due to the deposition and lift-off of electrodes. Nevertheless only using the lowest order resonances for driving is limiting as these are the slowest responding

modes. Multiple larger order modes are available thus it is worth to investigate if they can reproduce similar switching at faster rates. By applying a white noise signal on the structures all different optically active mechanical modes can be seen from the resulting spectrum when performing a PSD measurement. [28]

From a PSD measurement all the optically active modes should be visible. There are however further modes of mechanical oscillations. Numerous modes will have out of plane motion which will likely not produce any visible effects in coupling between the waveguides, as they will approximately be at the same distance from each other. The optically active modes can be analyzed by setting the sinusoidal drive to match the frequencies which are found from the mode analysis (at half the frequency that is). An interesting question for this approach will be whether or not each of the devices will show 6 individual modes for all of the different resonances, 2 for each of the cascaded devices, and if this limits the response when driving on the resonant frequencies.

The advantages of driving resonantly, possibly finding the responding modes with the largest frequency will be that the devices can switch extremely fast. On top of this it will require much lower voltages for the same amount of switching, thus a lower power consumption. This occurs as the amplitude of the oscillations will scale proportional to  $A \propto Q$  where  $Q$  is the quality factor of the individual modes [29]. This statement will be true as long as we are driving the devices exactly on the resonance frequency. As the linewidths of the structures are usually around  $\approx 1$  [kHz] which is the same as the resolution used on the function generator, we will at worst be at the point of FWHM, thus the amplitude will be lowered by a factor of 2 in such a scenario.

## 2.5 Chip design and experimental setup

### Chip and device design

Simulating a given geometry for the design is one thing on its own. These will serve as a basis for the geometry and properties of the active part of the system, including the size of the NOEMS and the properties of the electromechanical actuators as well. However this is not solely sufficient in designing the structures which are send for fabrication, as other factors needs to be included to ensure that the devices are fully functional. First of input gratings are necessary for the in coupling of the light. These furthermore serves the purpose of only coupling the TE-modes into the waveguides. On top of this it is needed to ensure that we are only in/out coupling from the grating that we intend. For this we need a spacing between the gratings of  $\approx 15 - 20\mu m$ , as this allow us to safely focus the laser at the intended port. In order to access all of the gratings in the designed device its a constraint that these are within the focus of the laser used for coupling, and the focus used for out coupling. This leaves us with the restrictions that all gratings in the system should be within  $\approx 60 - 80\mu m$  of one another. As the devices have a larger footprint compared to the previously designed NOEMS devices bending of the waveguides are required in order to include all gratings inside the desired area. This leads to longer waveguides and thus the requirement of extra tethers to support these suspended waveguides.

Furthermore we need to isolate parts with different electric potentials, this leads the use of trenches that are made between the different parts which are electrically active. Finally trenches and waveguides will lead to undercut areas around them, this restricts how closely each of these elements can be placed in the structures and it is ultimately a limitation occurring in the fabrication process. For the single beamsplitter/phaseshifter

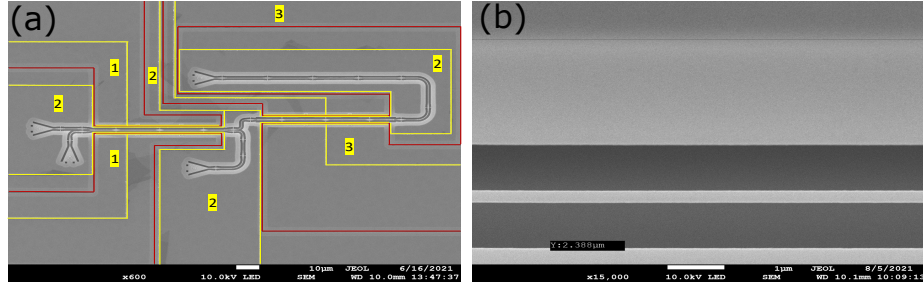


Figure 2.8: **Geometry of the full unitary along with the undercut** (a): SEM image of the full unitary device complete with trenches (red) and electrodes (yellow). The numbers denote the different potential regions which are isolated from each other through trenches. Both of the actuations (1) and (3) shares the same ground potential (2). All the electrodes are connected to the bonding pads outside this SEM-image (b) Showing the undercut in this case  $2.8\mu\text{m}$ . This restricts how closely the trenches and waveguides can be located in order to ensure stability of the device.

designs this has already been made which ensures that all of these problems are solved at once, the only difference for these structures is the bending of waveguides bringing the gratings closer.

However for the full unitary operation, 2 separate electrical parts are necessary, thus requiring further trenching and considerations. This proves to be an issue for the standard way of designing the structures, where 2 large bonding paths are simply placed on either side of a row of devices in order to give the potential difference over the device, allowing actuation. In this case however, at least 4 bonding pads are needed for each device to obtain the 2 potential differences. This leads to complications for the trenches and the wiring as the current technology does not allow for electrode/electrode, trench/electrode or electrode/waveguide crossing. Furthermore all the trenches needs a certain spacing given by the undercut in the fabricated structure. A novel design is thus presented which allows for all of the criteria to be met, thus giving a functional device that is not collapsing under fabrication. This geometry is shown in figure 2.8. Here the electrodes and trenches are highlighted.

It is important to note that while this design allows for 2 separately actuated devices it is not compatible with further upscaling of a potential network based on these structures. To realize a network capable of more than a  $2 \times 2$  operation, electrode, trench and waveguide crossing needs to be realizable in the fabrication process. On top of this the inclusion of direct fiber coupling might simplify the design. With this said and done this does allow for the proof that 2 devices can be actuated separately.

## Experimental setup

The same setup on the optical table was used for all measurements done during the project. The only difference being how much of the setup was actually utilized. The basic principles was 2 inputs and 2 outputs from the same incident laser. This is separated into 2 different paths corresponding to the input gratings. The cryostat ensures that there are no back reflections which is sent to a camera allowing us for optimal alignment to the gratings. Aligning near perfectly is ensured by having the light passing through a set of mirrors that allows for beam walking with 4 independent controls corresponding to moving the beam up/down and left/right on the chip. Optimal alignment is obtained by having a

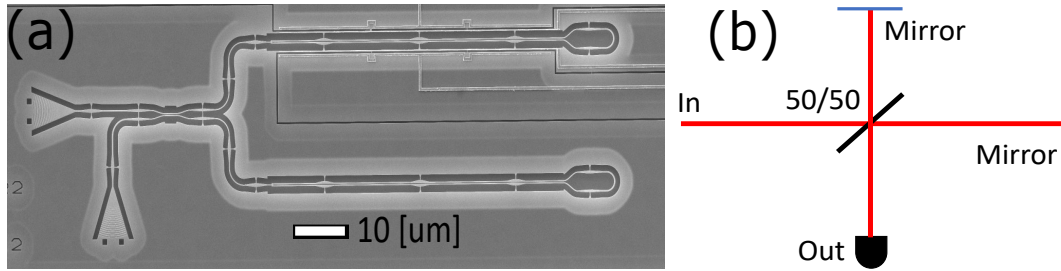


Figure 2.9: **The setup for the symmetrically based phase shifter** (a):The symmetrically based phase shifter, here one grating is used for the input and one grating is used to collect the results. Both of the interference arms has a MEMS device in order to balance losses, however only one arm can be actuated. (b) Sketch of a Michelson-Morley interferometer which compares to the setup. Actuating the device should lead to a sine wave response which depends on the voltage.

near Gaussian mode allowing for the largest possible coupling to the TE-modes generated by the gratings. Furthermore a set of polarizers is used in each of the arms to match the polarization of the gratings which is determined by their orientation. The same method is used after out coupling from the gratings on the other side of the device. Here the coupling is ensured by attaching the laser to the outputs where the detectors will be situated during the actual measurements. With this method the light is coupled in the same manner by using the resulting image from the camera that is connected to the setup.

### Symmetrical phase shifters - chip design

For the phase shifters that are build on the principle of utilizing the symmetrical pumping and shift in the effective index for the symmetrical mode we are using a novel design. It would be possible to simply include this phase shifter in a Mach Zehnder like setup. However this device also allows for another method where an interferometer is build on chip, thus the measurement does not require any out of chip complications in the setup. This is done by using a 2 port circuit on the device in a Michelson Morley type interferometer. This ensures that the phase shift effects can be directly measured from the output signal intensities. This can be seen in figure 2.9.

### Devices analyzed

Different kinds of structures were analyzed during this project. In the beginning structures designed by Sif were analyzed [24]. This was primarily to get a feeling of the experiments needed to be done. These devices were designed asymmetrically on purpose to study the phase effects, furthermore they were not cascaded, instead only a single device was in each of the individual structures similar to [7]. This lead to the conclusion that longer devices were needed in order to achieve a full  $2\pi$  phase change between the arms. On top of doing the regular phase and switching measurements on these devices, the focus was on the mechanical responses, including switching speeds, noise and the mechanical resonances in the system, completed in order to get a better understanding before moving towards the more mechanically complicated cascaded structures. Only the results of the mechanical properties are reported here, as the phase shifting effect was improved via my own devices.

Afterwards the novel architecture including cascaded NOEMS devices was analyzed, here the focus was again on phase change, switching and the mechanical properties of

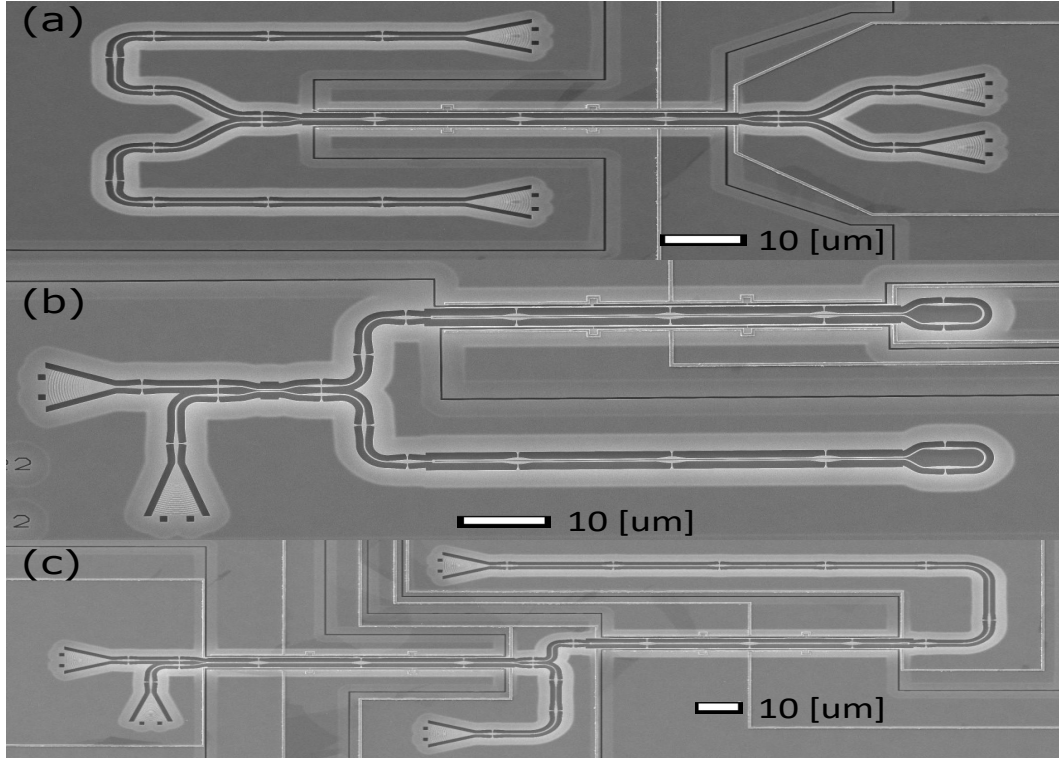


Figure 2.10: **The setup for the symmetrically based phase shifter (a):**The switch/asymmetrically based phase shifter with 2 inputs and 2 output ports(b) The symmetrically based phase shifter in the Michelson-Morley type setup (c) Full unitary, including both the switch and the symmetrical phase shifter.

the devices. These are the cascaded devices, designed for larger effects, while maintaining similar mechanical properties, such as switching speed and stability. Mainly 2 different samples were analyzed, the first one turned out to have narrower features in all of the waveguides compared to the original design. Only the intended tuneable beamsplitters could be analyzed in this sample. Another sample was created where all the waveguides were intentionally designed to be broader than what was desired in order to mitigate the fabrication issues. This gave waveguides with similar properties as what was initially intended. Here all the 3 different devices could be analyzed. The 3 kinds of devices that is analyzed through this project is shown in figure 2.10

### Experimental Setup and measurement theory

All results reported in the following was obtained by measurements using the same Flow cryostat. A couple of different experiments were carried out using the same optical setup utilized in different ways.

The tuneable splitting ratio measurements and all measurements of the mechanical properties of the system required a similar optical setup. Here only one input port is excited, and light is collected from both output ports. For the tuneable splitting ratio this is then reproduced where the other input port is excited, in order to observe effects from both arms. In every experiment the output is collected by photo detectors connected to an oscilloscope. The alignment and phase settings of the 2 output ports are set in such a way as to optimize the signal of both outputs.

Estimating the tunable beamsplitting ratio requires a 4 port measurement. This is to eliminate in and out coupling efficiencies which might vary over the 4 input/output ports. Labeling the 4 ports with  $i=1,2,3,4$ , where 1 and 2 are the input ports and 3,4 are the output ports. A CTL laser is focused on one of the input ports, 1 or 2, at a locked wavelength. The output is then collected at both 4 and 3 simultaneously. The measured intensities in the output ports are then given by the transformation

$$\begin{pmatrix} I_{out,3} \\ I_{out,4} \end{pmatrix} = \begin{pmatrix} \eta_1\eta_3T & \eta_2\eta_3R \\ \eta_1\eta_4R & \eta_2\eta_4T \end{pmatrix} \cdot \begin{pmatrix} I_{in,1} \\ I_{in,2} \end{pmatrix} \quad (2.35)$$

The  $\eta_i$ 's are the different grating efficiencies, T and R are then the transmission and reflection coefficients of the gap variable directional coupler which are grating independent. These are voltage dependent and will be changed given the actuation over the NOEMS. By matching the input power in either port 1 or 2, or normalizing these compared to each other a measurement of either  $I_{ji} = \eta_i\eta_jT$  for the ports connected to the same waveguide, and  $I_{ji} = \eta_i\eta_jR$  for cross port coupling, can be obtained. From this the splitting ratio between the ports can be estimated as

$$SR = \sqrt{\frac{I_{31} \cdot I_{42}}{I_{41} \cdot I_{32}}} \quad (2.36)$$

This is independent of the in/out coupling efficiencies of the gratings. Furthermore the efficiencies of the out coupling gratings can be estimated by using that

$$\frac{\eta_4}{\eta_3} = \sqrt{\frac{I_{41} \cdot I_{42}}{I_{31} \cdot I_{32}}} \quad (2.37)$$

This value should be constant over the different voltage settings, at least when looking at a region far from the largest splitting ratio where the values will fluctuate more and be less precise.

For phase measurements on asymmetrical devices more sophisticated methods has to be utilized in order to estimate this as a function of the applied voltage. A simple Mach-Zehnder-like setup is not sufficient in the case of the phase-splitter devices. Here we will also see tunable splitting effects, thus a measurement independent of the varying splitting ratio has to be conducted. One method is to have a setup as shown in figure 2.11, where both input arms are pumped at the same time, on top of this an external phase shift is applied to one of the arms with a tunable Piezo mirror capable of changing the phase  $2\pi$  between the arms [30]. When doing this without actuating the waveguides the resulting output measurement will be a sine wave as the external phase shift is scanned via the Piezo mirror. This is due to interference between the 2 input arms in the directional coupler. When actuating the NOEMS 2 different scenarios are possible. If the devices are perfectly symmetrical the amplitude of the sine wave will shrink, until the entire sine wave flips, corresponding to the voltage where light is switched between the output ports, a conceptual sketch of this effect is seen in figure 2.12.a, here different voltages are applied (0V (black), 4V (blue) and 7V(red)). It can be seen that the applied voltage only changes the amplitude as the external phase is scanned over time, until the point where the switching is complete, here the phase changes by  $\pi$ . In the case of asymmetry this effect will also be seen, as the tunable splitting ratio is still changed with the varying voltage over the NOEMS. However, in this case the phase will also be changing at the output port which is measured. This will result in a shifting of the sine wave, from which the imparted phase change as a function of the applied voltage  $\phi(V)$  can be extracted. A conceptual sketch of this effect is seen in figure 2.12.b, here different voltages are applied (0V (black), 4V (blue) and 7V(red)). Here it is seen that the applied voltage changes both the amplitude

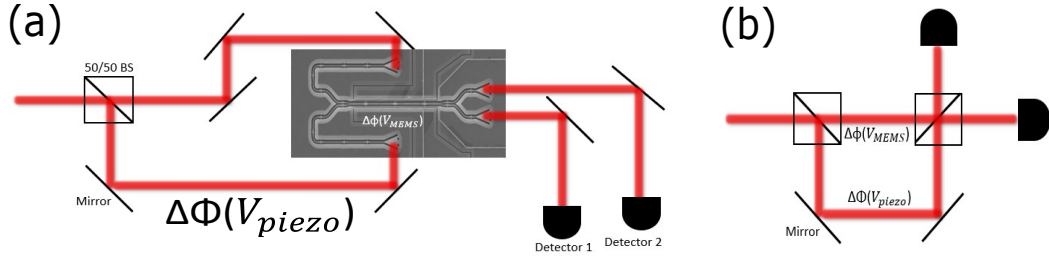


Figure 2.11: **Conceptual sketch of the asymmetrically based phase shift measurement** (a): Full conceptual sketch of the phase shift measurement, where a Piezo mirror is used as an external phase shifter on one of the input arms in the setup (b) Simplified sketch of the same setup, showing that the principle is a Mach-Zehnder type interferometer where 2 phase shifts can be applied in the setup.

and phase offset of the corresponding sine wave that occurs when scanning the external phase over time.

When carrying out this experiment the effects of drifting also has to be taken into account. Drifting in the setup might cause the sine wave to shift when measurements are taken at different times. This will likely be occurring at a time scale of seconds or minutes. Thus it is beneficial to carry out a measurement at the 2 different voltage settings simultaneously in order to minimize the effects of drifting. Luckily this is possible with the function generator, allowing us to input a specific function at a frequency which is much faster than the time it takes for the external phase shifter to scan through the entire applied phase range. By saving the actuation signal on the NOEMS, corresponding to the on/off switching of the devices, along with the measured data this can be used to mask the data in order to get 2 sine waves from a single measurement. These 2 sine waves will correspond to the one at a set voltage, and a sine wave at 0 voltage used for reference. With this method the effect of drifting should be negligible and the sine waves can be readily fitted in order to extract the phase difference between the waves, which will simply be in the form of an offset. The resulting data is fitted with.

$$f(x) = a + b \cdot \sin(c * x + off) \quad (2.38)$$

Here the different constants  $a$  and  $b$  are not of importance, as they depend on the tunable splitting ratio, which is extracted using other methods anyway. The important point is that for the 2 fitted curves the speed of the sine wave  $c$  has to be fixed. When this is met, the difference in the off values when fitting the sine waves gives the phase change induced on that arm.

When doing measurements in order to analyze the mechanical properties of the devices, such as the mechanical resonance frequencies, the change in resonances due to actuation and noise in the devices, we are carrying out noise Power spectral density (PSD) measurements [28]. This is a measurement on how the power of the measured signal is distributed over frequency. Here a continuous laser signal is sent through the devices, and by performing Fourier transforms we are able to see the frequencies of mechanical responses as peaks in the PSD spectrum in a given bandwidth, this process is carried out directly through the oscilloscope when collecting the measurements. This allows for estimation of the mechanical properties of the system, including noise ratios occurring due to oscillations of the waveguides. In order to minimize the noise arising from the detectors themselves a low pass filter was introduced at  $\approx 5$  MHz as the mechanical resonance frequencies of inter-

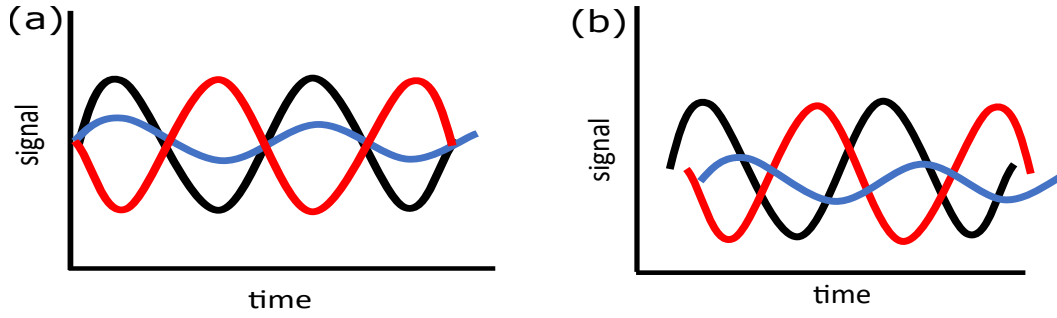


Figure 2.12: **Conceptual sketch of the responses in the phase measurements** (a): The expected response of a completely symmetrical system, here no phase shifting of the sine wave occurs at the different voltages (0V,4V,7V) Here it can be seen that only the amplitude is changing, until the point where a  $\pi$  phase shift is occurring at the point where the output signal is completely switched (b) Signal of the same measurement now with asymmetries in the waveguide widths. Here it can be seen that there is a shift in the sine wave along with a change in the amplitude. This corresponds both to a shift in the  $\theta$  and  $\phi$  when mapping the response to the Bloch sphere.

est in occurs at lower frequencies. When performing PSD measurements and subsequent analysis it is important to disregard artifacts arising from the laser itself, or other sources not being a part of the NOEMS devices. The actual mechanical responses will show as Lorentzian responses on the form [27]

$$f(\omega) = \frac{1}{\pi} \left( \frac{\gamma}{(\omega - \omega_0)^2 + \gamma^2} \right) \quad (2.39)$$

Where  $\omega_0$  is the resonance frequency and  $\gamma$  is the full width half maximum. From this the quality factor (Q - factor) is defined as [31]

$$Q = \frac{\omega_0}{\gamma} \quad (2.40)$$

Which is a measure on the amount of oscillations before dampening. Furthermore this serves as a measure on how much the system will respond if it is driven at its resonance frequency.

Finally when noise of the devices are of interest it is important to note that there will be different noise levels depending on the tuning setting. Devices that are capable of producing a full switching between the output ports will have vastly different noise responses. This is the case as at either maximum or minimum intensity small fluctuations in the position of the waveguides with respect to each other will not have a large impact. In general the noise level is dependent on the slope of optical response as a function of small changes in the position corresponding to said result. As the response goes as  $\cos^2(V^2) \propto \cos^2(d^2)$  where  $d$  is the distance between the waveguides, it is evident that the slope is largest in the region where the corresponding output signal is 50/50. Thus when doing noise measurements we are able to set a maximum value of the expected noise in the system, by first scanning all voltages, then parking at the 50/50 setting and performing the aforementioned PSD measurement we are able to extract the maximal amount of noise.

### Optimal waveguide geometry

Numerous considerations has to be taken into account when designing the optimal structures, this is mainly related to the widths of the waveguides constituting the devices,

both for the symmetrical and asymmetrical cases.

One important aspect is that the waveguides should be working in the single mode regime, such that they need to be narrow enough as to only support the lowest order TE-mode (They will also support a TM-mode, however gratings assure that these are not excited). This requires these GaAs waveguides to be narrower than  $\approx 250$ [nm]. Furthermore the system works on the principle of the modes being evanescent, evidently from figure 2.4 broader waveguides will confine a larger amount of the mode compared to a narrow waveguide. Thus narrow waveguides will require shorter propagation lengths in the active area, or a lower applied voltage resulting in smaller gap differences when actuating, as with these waveguides the resulting overlap integral with a nearby waveguide is larger. On the flipside these modes have larger slope in the effective refractive index  $\Delta n_{eff}$  for small variations in the waveguide widths  $\Delta w_{gwidth}$ . From figure 2.4 it can be observed that this is a factor of 2 from a width of 190 [nm] to a width of 225 [nm]. In the perfect world this is not an issue, however when fabricating the structures there might be fabrication errors. One of these comes in the form of surface roughness, causing different parts of the waveguides to have different widths. A waveguide with a larger  $\Delta n_{eff}$  around the mean width will experience larger losses due to surface roughness, as a larger part of the light is confined outside the waveguide and will scatter from said roughness. [20]

Another consideration when designing the samples is the initial gap between the waveguides  $d_0$ . Ideally we want the gap as small as possible, as this is the region where  $\Delta g$  for varying gaps is found, thus creating the largest optical effects. which is evident from figure 2.5. There is however a fabrication constraint on what can be realized. If the gap size is made to small the parallel waveguides will snap to each other under fabrication. Previous similar structures, without cascaded sections, could be fabricated with large success with gap sizes in the order of 100[nm] [7]. It did however turn out that for these cascaded structures the survival rate was larger for gap sized above 120[nm]. This was thus used in every sample apart from the first one where this was discovered.

### Fabricational limitations

As previously mentioned when dealing with actually fabricated devices the world is no longer as perfect as when simulated in COMSOL. Numerous effects has to be taken in to account as we desire to have functioning structures that are not collapsing under fabrication. Firstly, in the optimal case the initial separation between the waveguides  $d_0$  should be as low as possible, as the coupling between the waveguides  $g_0$  and the change in this when actuating are largest in this regime. This is however limited by fabrication, here we observed in the different structures that an initial gap  $d_0$  of at least 120 [nm] was required in order for the devices to not collapse, and even in this region the success rate was not ideal. This sets limits on which simulations are actually useful to carry out, as we desire to simulate a realistic device.

Another error, which was evident from the SEM-imaging done on the structures after fabrication, was changes to the parameters that were initially intended. Most notably the waveguides turned out to be significantly narrower than designed in the mask, in the order of  $\approx 30$ [nm]. This resulted in larger losses, due to surface roughness as explained in section 2.2. Furthermore this seemingly increased the gap size compared to the initial design, thereby leading to effects differing from the simulations. An analysis of the SEM images where carried out with the aim of estimating the actual differences from the design itself. By taking the line cut of the waveguides at all different x positions, the direction along the waveguides, on the 2 waveguides, the widths and the gap size can be determined. This is

shown in figure 2.13 and figure 2.14. These results lead to the fabrication of a new sample, where all the widths in the design mask were increased in order to obtain the desired waveguide widths, the corresponding result is shown in figure 2.15. Thus we will analyze 2 different samples with varying waveguide widths and levels of asymmetries throughout this work.

Furthermore this analysis allows for an estimation of the waveguide roughness. As the resolution on the pixels are  $\approx 1\text{nm}$  it is clear from the uncertainty on the widths that we are seeing surface roughness as we are seeing larger discrepancies than single pixels. This is crucial as the surface roughness will lower the power transmitted through the waveguides as it will give more scattering, especially when the waveguides are narrower than intended.

Finally both samples analyzed in figure 2.14 and figure 2.15 were meant to be devices with a symmetrical structure. Evidently from the figures and the width estimation it is clear that there is a discrepancy between these widths - giving asymmetrical structures. In the case of the first chip design the 2 widths were estimated to be  $190 \pm 2\text{ nm}$  and  $186 \pm 2\text{ nm}$ , thus a discrepancy of more than  $2\sigma$ . Whereas in the second chip design the widths are estimated to  $210 \pm 3\text{ nm}$  and  $213 \pm 3\text{ nm}$ , this time the discrepancy is within  $1\sigma$ . This will prove to be quite a limiting factor for the system, as we are seemingly not able to create symmetrical structures at all. The effects of these, albeit small asymmetries, will have an impact on the results. This will specifically be in terms of phase shift and the inability to perform 100/0 switching. Previously when devices with tunable splitting ratio capabilities were constructed, the effects of these inevitable asymmetries were not analyzed in greater detail. This will thus be a further exploration both in terms of the change in mechanical modes and the optical response of actuation. Furthermore as the waveguides initially turned out to be narrower than intended, the widths are in a region with a larger  $\Delta n_{eff}$ , this means that even small variations in the actual widths will lead to a larger asymmetry in the propagation through the different waveguides giving a greater phase shift than for broader waveguides with similar relative variations in the width. In addition it is also unclear how much the symmetrical phase shifter is affected by this. Finally the narrower sample has a larger uncertainty ascribed to the width estimation which corresponds to increased surface roughness on the waveguides, this will impact the amount of losses. This is an issue as these effects are even stronger in this region due to a larger  $\Delta n_{eff}$ . Thus the first sample is expected to have a greater amount of losses.

Another very curious result is that there is such a large discrepancy between the gap sizes in the 2 different samples. Here it is evident from the figures that the first sample has a gap of  $173 \pm 4\text{nm}$  where the second sample had a gap of  $127 \pm 2\text{nm}$ . This will likely impact how well coupled the waveguides are to each other and how much this can be changed by moving them via actuation. However it is the narrower waveguides, having larger portion of evanescent mode which also has a greater gap, this will oppose the effect of larger gap sizes.

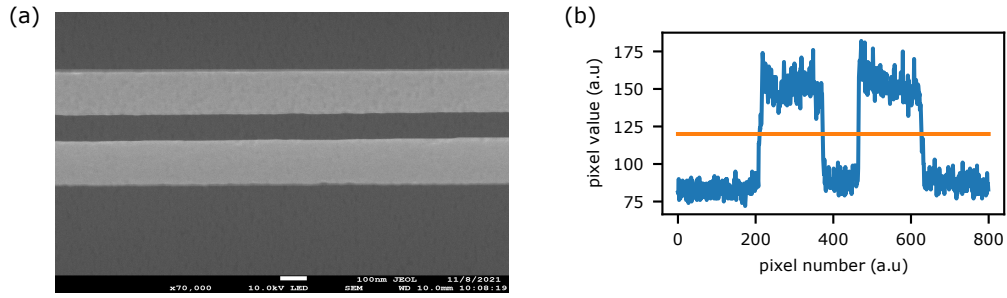


Figure 2.13: **SEM images and line cut for analysis** (a) SEM image of parallel waveguides in the directional coupler. (b) Pixel values of vertical line cut of the image. Here waveguides can be seen with larger pixel values, while the gap is between them. A threshold is set to analyze the waveguides widths, by using the scale provided in part (a). The extracted widths converted to nm can be found in the following figures

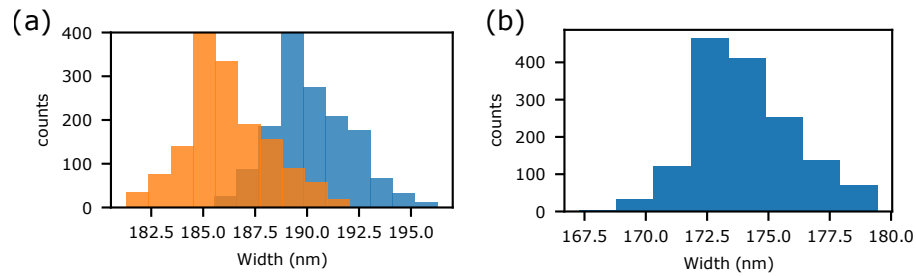


Figure 2.14: **Results for analysis of the initial waveguides and gap over the length** (a): Widths of the 2 waveguides. Waveguide 1 (blue) has a width of  $190 \pm 2(nm)$  whereas waveguide 2 (orange) has a width of  $186 \pm 2(nm)$  (b) analysis of the gap between the waveguides yielding  $173 \pm 4nm$

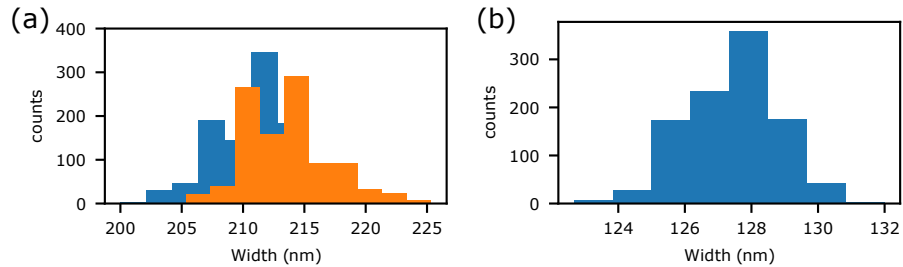


Figure 2.15: **Results for analysis of the corrected waveguides and gap** (a): Widths of the 2 waveguides. Waveguide 1 (blue) has a width of  $210 \pm 3(nm)$  whereas waveguide 2 (orange) has a width of  $213 \pm 3(nm)$  (b) analysis of the gap between the waveguides yielding  $127 \pm 2nm$

## Part III

# Experimental results

# Chapter 3

## Results

In the following section results of various experiments are reported. Here the optical responses are shown first, including symmetric/antisymmetric based phase shifts, tunable switching ratios and the effort of doing a full unitary operation. Afterwards the results from the mechanical studies are reported, specifically the resonance frequencies along with quality factors, maximum noise levels and resonant driving of the system. Finally the response from the MMI's located in the phase shifters based on symmetry is shown.

### 3.1 Phase shift measurements

The method for conducting the phase shift measurements are described in section 2.5. Due to mechanical resonance frequencies a well tailored function has to be utilized when actuating the devices. It is desired to not induce oscillations in the system, while still maintaining a large dialing speed of operations. Evidently from figure 3.1 instant switching induces a wildly oscillating response. Through trial and error we arrived at the Tukey drive as the best function for actuation. A tukey window (cosine tapered window) is thus applied over the NOEMS on the form

$$\begin{aligned} w[n] &= \frac{1}{2} \left[ 1 - \cos\left(\frac{2\pi n}{\alpha N}\right) \right], & 0 \leq n < \frac{\alpha N}{2} \\ w[n] &= 1, & \frac{\alpha N}{2} \leq n \leq \frac{N}{2} \\ w[N-n] &= w[n], & 0 \leq n \leq \frac{N}{2} \end{aligned} \quad (3.1)$$

The frequency of the Tukey drive applied over the NOEMS was chosen to ensure that the mechanical modes of the waveguides were not excited, in order not to start oscillations. Thus we needed this to be slower than  $\approx 1\mu s$ . Different arbitrary Tukey drives can be seen in figure 3.1. Here it is important to note that changing the value  $\alpha$  ultimately changes the rise time of the function, which is the limiting factor. Furthermore for phase shift measurements we were interested in scanning the voltage applied to the external Piezo mirror fast enough to not see any effects due to drifting over the time period of a single full  $2\pi$  Piezo scan. On top of this we ensured that this was still significantly slower than the NOEMS actuation, to ensure sufficient statistics were achieved for the fitting of the sine curves. The on/off signal over the NOEMS, corresponding to when the system is switched can be seen in figure appendix A.1. This data is used to mask the obtained data, such that it can be split into the 2 sine curves.

Figure 3.2 show the raw data taken from a phase measurement. Here it can be seen that the Piezo is doing a full scan in  $\approx 10[\text{ms}]$ , this was evidently sufficient for drifting effects to be negligible, and was primarily found via trial and error of different speeds. The resulting figure only show the data from the reflection port. In figure 3.2 a zoom on part of this data can be seen. Here the on/off switching via the Tukey drive is evident.

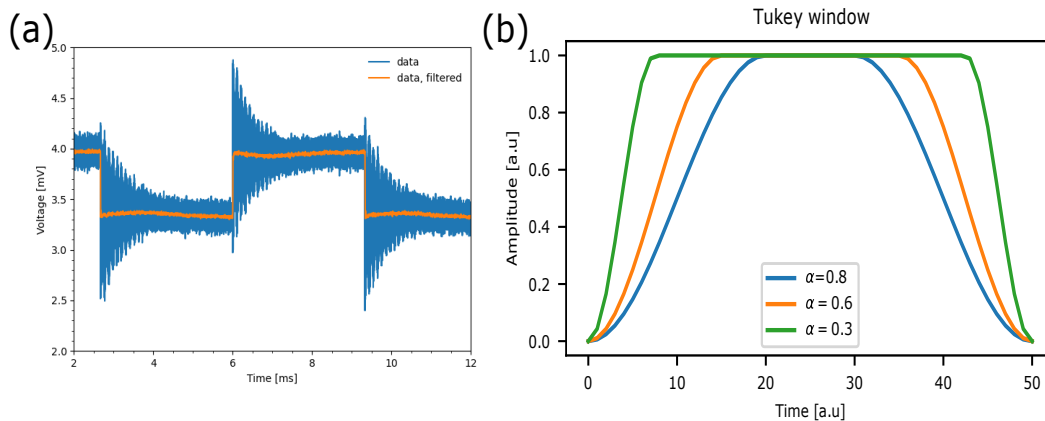


Figure 3.1: **Instant switching and the tailored tukey drive for actuation:**(a) example of instant switching of the NOEMS voltage setting. Here clear oscillations are seen which slows down switching rates (b) Examples of different tukey drive, here we can tailor the switching speed making the rise time just below that of the resonance frequencies, thus not inducing oscillations

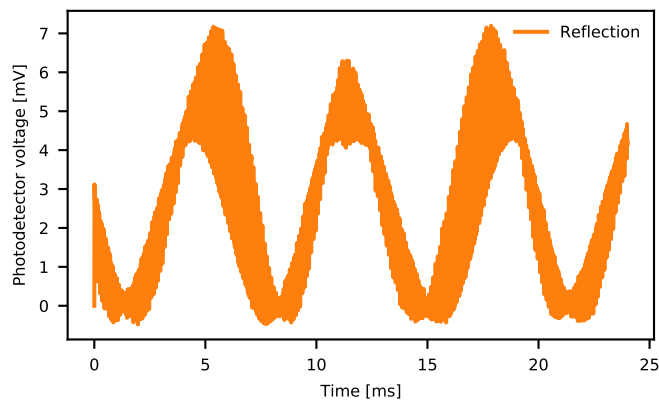


Figure 3.2: **Full Phase shift scan at 4V actuation:** The Externally applied phase from the Piezo is done with a ramp, while the NEMS is switching with a period of  $\approx 1\mu s$ . The resulting phase change can be observed by the shift of the 2 sine waves, corresponding to the voltage over the NEMS being switched on/of. The abrupt changes occurs when the piezo ramp changes direction, this is with a period of  $\approx 10ms$ . By cutting the data within 1 period of the piezo scan, 2 sine waves can be fitted to the data. These should evolve with the same frequency, however they will be shifted with a phase which gives the phase shift induced on the output port.

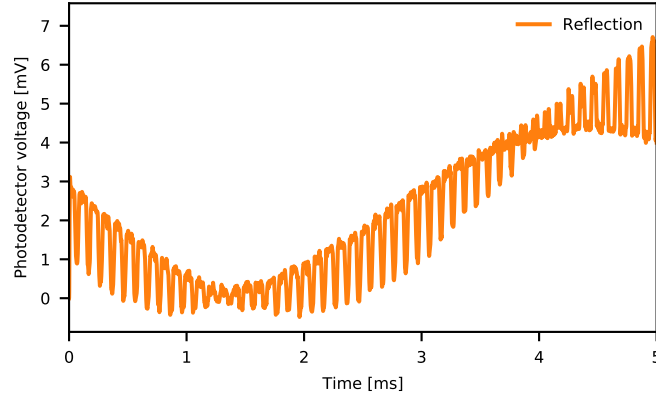


Figure 3.3: **Zoom in on phase shift scan, actuation of 4V**: Zoom in on 5 ms of the scan shown in figure 3.2. Here the distinct difference between the 4V applied on the NOEMS and 0V applied on the NOEMS can readily be seen by the peaks.

The masking process is carried out with boolean operations in python, the corresponding signal used for the masking process can be found in Appendix A.1. Here it is however important to note that the switching is not instant, meaning that all points in the mask will not correspond to the actual value after the system has settled in the new position. In order to overcome this, only the last couple of points either in the on or off, before the switching back is being used for the data shown in figure 3.3-3.6. This ensures that the system has stabilized fully.

The resulting sine curves extracted for numerous different voltages are seen in figures 3.3 - 3.6. Here it is evident that the red curve is fixed, up to small amounts of drifting occurring as the different data sets were taken at different times. The red curve corresponds to no actuation of the devices. As stated the important aspect is only the difference between the 0V case, as reference, and the voltage in question in each of the figures. Thus this drifting between the different data sets is not an issue, as the reference will have drifted the same amount. Furthermore the time scale is set to start from 0 for the cut out part of the data.

By extracting all of the fitted values, the phase shift for each of the voltages applied can be found and plotted as a function of  $V^2$ . The reason to plot it as a function of  $V^2$  is that the displacement is changing as a function of this. Thus a voltage change at larger voltages has a greater impact than a similar change at low voltages.

The total resulting phase change is seen in figure 3.8. The maximal achieved phase change is close to  $2\pi$ , as the total achievable phase range from 0V to 7 V is  $\phi(V) \in [0, 1.94\pi]$ . Furthermore the theoretical pull in voltage of the devices is  $\approx 12V$  meaning that it should be possible to reach the full required phase range with these devices by simply turning up the voltage range applied slightly. The drawback is of these devices however, as mentioned in section 2.2, is that there is also switching of light simultaneous to the phase changes, thus we also need to analyze this switching to determine the full imparted rotation on the Bloch sphere.

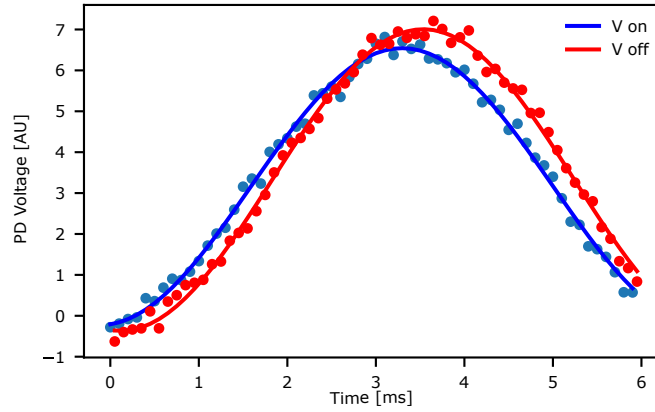


Figure 3.4: **Sine fits to data with no actuation and actuation of 2V**: The points corresponding to V off and V on are found by the mask made from the data in figure 2.5. This results in a phase shift of 0.22 [rad]

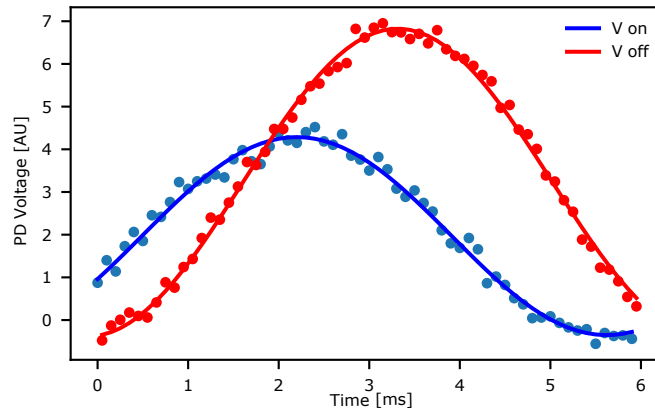


Figure 3.5: **Sine fits to data with no actuation and actuation of 4V**: The points corresponding to V off and V on are found by the mask made from the data in figure 2.5. This results in a phase shift of 0.54 [rad]

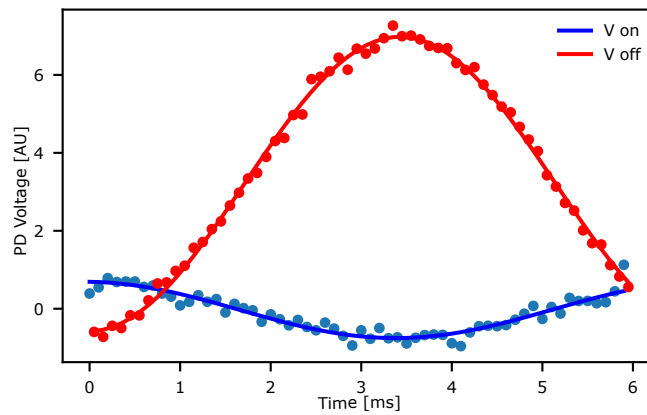


Figure 3.6: **Sine fits to data with no actuation and actuation of 6V**: The points corresponding to V off and V on are found by the mask made from the data in figure 2.5. This results in a phase shift of 3.05 [rad]

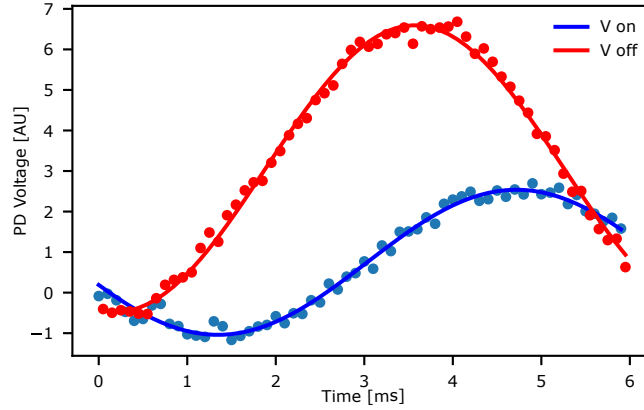


Figure 3.7: **Sine fits to data with no actuation and actuation of 7V**: The points corresponding to V off and V on are found by the mask made from the data in figure 2.5. This results in a phase shift of 6.5 [rad]

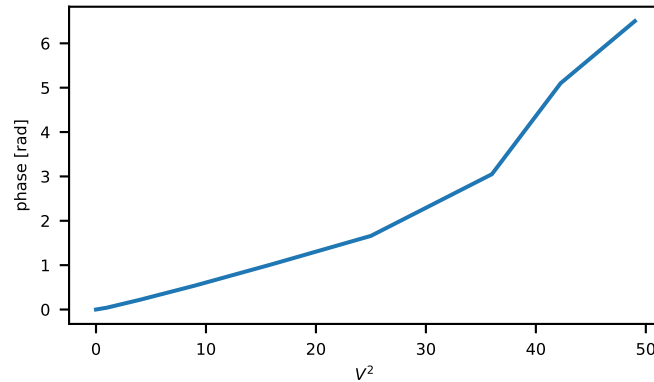


Figure 3.8: **Total phase shift as a function of  $V^2$** : Phase shift as a function of the Voltage squared. It is evident that the phase change induced increases rapidly with larger voltages. An applied voltage of 8V should thus be sufficient to perform the full  $2\pi$  rotation in the phase direction on the Bloch sphere

## 3.2 Switching capabilities

The aim is to fully characterize the 2 rotations on the Bloch sphere  $\{\theta(V), \phi(V)\}$  impeded by the device. Previously the phase range was characterized, now the  $\theta(V)$  will be determined, corresponding to the switching abilities. As this device has shown the capabilities of producing a full  $2\pi$  phase shift, at least if we go voltages slightly larger than those used in the experiment, the main usability of this device will not be that of a switch but instead a phase shifter. As the device is asymmetric it will likely not be able to produce a great splitting ratio. However if this device were to be added in succession with a symmetric device, functioning solely as a switch, a full arbitrary rotation on the Bloch sphere is possible.

The experimental method is described in section 2.5. A single input is used in port 1, and the resulting output is measured in the transmission and reflection ports. Meanwhile the ramp signal is saved, as we desire to observe the effects from a single ramp. The full results are seen in figure 3.9. Notably the ramp is applied over 1 ms, the 0 voltage is in the middle of the shown ramp on/off "heaviside" functions. In this data the background

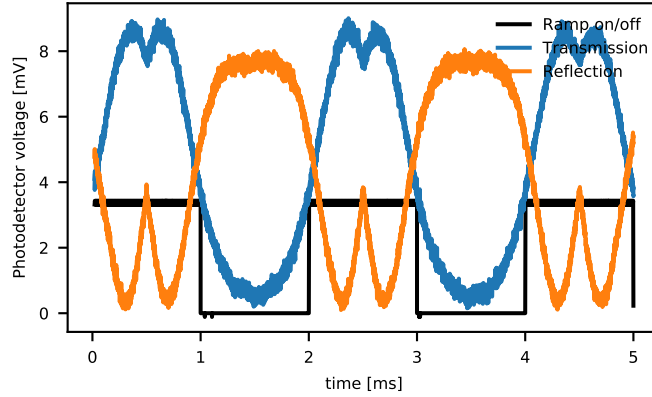


Figure 3.9: **Switching between 2 output ports with a single input port being excited:** A single input waveguide is excited and the resulting transmission and reflection is collected from the 2 output arms. This is tuned with a ramp signal applied on the NEMS. The on/off periods of the ramp, corresponding to the ramp going up and down is shown (black). The central points are the turning points for the direction of the ramp. The ramp is driven from 0V to 7 V

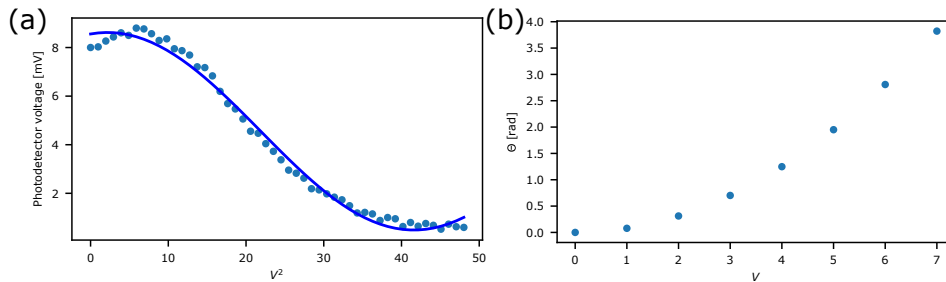


Figure 3.10: **Sine Fit to a single ramp of switching from 0V to 7V applied** **CHANGE LABEL:** A cutout of the time period for a single voltage ramp from 0V to 7V applied on the NEMS. A sine curve is fitted to the data to find the speed of the oscillation. From this the total rotation on the Bloch sphere, in the switching direction can be estimated.

noise has been subtracted from the measurements at the output ports. This background noise is found by performing a measurement where no light is inserted in the system.

From this data the time to complete a single ramp is cut out and is fitted with a  $f(\theta) = a \cdot \cos^2(\theta_2)$ . Notably when converting to the Bloch sphere  $\theta = 2\theta_2$  [32]. As the ramp is linear it is possible to convert the time into the voltage applied at that instance. This allows for a full description of  $\theta(V)$  to describe the rotation impeded on the Bloch sphere. A single ramp taken, for one of the inputs, can be seen in figure 3.10. Here it is evident that more than a full switching is occurring over the voltage range form 0V to 7V. Here the resulting rotation on the Bloch sphere in this voltage range is found to be  $\theta(V) \in [0, 1.24\pi]$  after converting to Bloch sphere rotation  $\theta$

### Full Bloch sphere rotation

As the parameters  $\phi(V)$  and  $\theta(V)$  has been estimated for discrete voltages between 0V and 7V, it is possible to evaluate the full rotation that this device is capable of on the Bloch sphere. This rotation is seen in figure 3.11. It is evident from the estimation of the

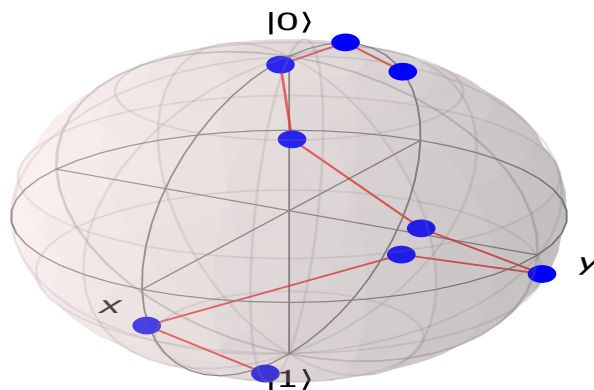


Figure 3.11: **The resulting rotation on the Bloch sphere from a single initially fabricated device operating between 0V and 7V:** The resulting rotation on the Bloch sphere when operating between 0 and 7 V for a single 2x2 device. This device is not capable of only doing one of the rotations on the Bloch sphere as initially planned. Even though it makes a full rotation in both parameters it is also not sufficient for reaching any arbitrary point on the Bloch sphere.

2 parameters, that we are able to cover the full range needed in both parameters. However as the parameters are co-dependent it is not possible to reach any arbitrary point on the surface. In the ideal case any point on the Bloch sphere should be reachable with 2 devices, where we would be able to reach  $\{\theta(V_1), \phi(V_2)\}$ , where 1 and 2 denotes the voltages at the different devices. Instead we are in the situation where  $\{\theta(V_1), \phi(V_1)\}$  is reachable. Thus this device in and on itself is not sufficient to do any unitary 2x2 operation. It might be possible to do specific operations, but adding another device is necessary for any arbitrary 2x2 operation.

There are different ways in which the additional device could be functioning to obtain an arbitrary rotation. If we are either capable of constructing a device only doing a  $\phi$  or  $\theta$  rotation when actuated this will be sufficient along with the previously demonstrated device which does both rotations. The most plausible solution is to create a device with more symmetrical properties.

It might also be possible to reach any arbitrary point by solely using devices that does both rotations. If 2 devices could do rotations that were orthogonal to one another, then by simply considering a shift in the basis of the Bloch sphere it is evident that this should also be able to produce any arbitrary rotation. However as the changes in parameters  $\theta$  and  $\phi$  when actuating is non-linear, it might prove difficult to construct a device where the rotation is always orthogonal in 2 distinct devices. Furthermore the effects are varying over different structures, seemingly at random, which complicates this solution.

### 3.3 Symmetrical phase change

For the symmetrical phase change a simple setup was used as the interferometer was build on chip, as a Michelson Morley type interferometer, this setup is seen in figure 2.8. Thus one port was used for the input and one of the gratings was used as the output. Consequently we can estimate the applied phase change on one arm compared to the other directly from the output port

$$I = \cos^2(\Delta\phi/2) + C \quad (3.2)$$

with the addition of a term  $C$  arising from the initial beamsplitter not being perfectly balanced as a 50/50 splitter.

However as the phase change was lower than expected, it was difficult to tell how large the phase change actually was as we had no immediately clear way to estimate the maximal and minimal power to calibrate the phase changes in between. Instead we opted to use an approximate solution, which only worked for larger voltages where the phase change was actually evident in the devices. Here we simply fitted the function in order to find the approximate phase at the different voltages. The data that was analyzed is exemplified in figure 3.12, where it is evident that for low voltages, the signal to noise ratio is far too great to give any valuable results.

The final results are shown in figure.3.13. Here it is evident that this device is not sufficient as a phase shifter usable for the 2x2 unitary. The acquired phase shift furthermore needs to be divided by a factor of 2 in order to account for the light traveling through the NOEMS twice with the use of the mirror. There might be several reasons as to why the experimental response provides a significantly smaller phase shift than what was simulated in COMSOL. The simulations suggested that a device with these geometrical parameters would be able to do a full  $2\pi$  phase shift.

As has previously been discussed we are seemingly not able to fabricate the 2 parallel waveguides in a symmetrical manner for the devices. asymmetries in the waveguide system will limit how symmetrical the pumped mode will be. This will in turn lower the phase change that can be obtained. It is however not straight forward for us to rule this as the sole problem of the structures. Another aspect is the 50/50 beamsplitters used in front of the NOEMS. These might have a couple of different challenges associated, firstly they are designed as 50/50 beamsplitters based on COMSOL simulations, this might not be exact as we know there are fabrication changes to the structures, and as the optical properties of the MMI changes rapidly with an increase in either the length or the width of the structures. Consequently not only the symmetrical mode will be pumped in the system, but also some amount of the asymmetric, this will probably lead to increased losses and a much lower phase change as well, depending on how off the splitting ratio is from being 50/50. Again we have no way of measuring this splitting ratio in the circuits that has been build. Finally all optical structures has losses, however objects with sharper edges and thus abrupt changes to the optical properties will often lead to greater losses. The MMI's are an object of such kind as will be studied in the following section. Another note to this aspect is whether the MMI's have other kinds of unwanted responses, such as cavity effects which is discussed in greater detail by the end of this chapter.

### 3.4 Full rotation on width optimized devices

As was seen from the analysis of the waveguide dimensions the fabricated devices differed from the intended by  $\approx 30\text{nm}$ . consequently the optical properties of the waveguides are vastly different than those simulated, the most important being that there is a much larger  $\Delta n_{eff}$  for small variations in waveguide widths, this gives larger phase changes with the increased asymmetry, and will likely also influence the amount of losses, as surface roughness leads to more scattering in this case. Furthermore these largely asymmetric devices are not sufficient for reaching any arbitrary point on the Bloch sphere, we are thus

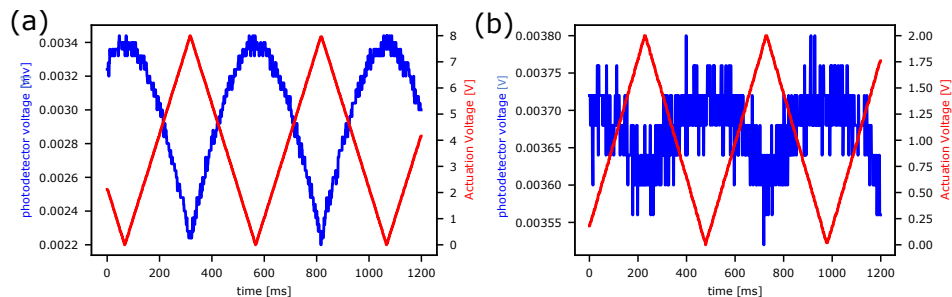


Figure 3.12: **Data from the symmetric phase measurements:** (a): photoelectric response (blue) from driving the actuation from 0 to 8 V with a ramp signal (red) Here a clear signal can be seen. (b): Photoelectric response when driving from 0 to 2 V. Here the signal to noise ratio prevents us from extracting valuable results.

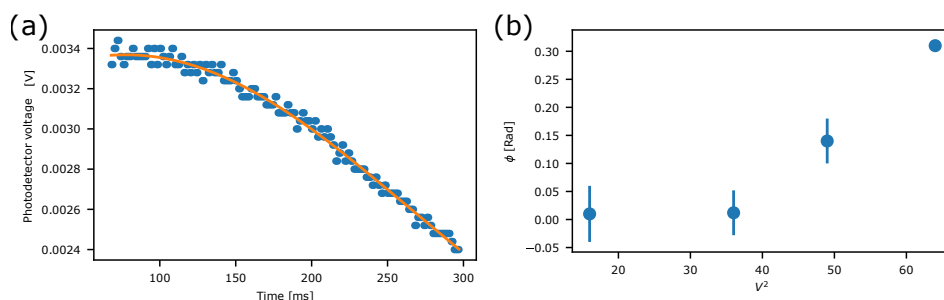


Figure 3.13: **Symmetric phase results:** (a) Fit to the response at an actuation going to 8V. This allows for extraction of the phase shift, in this case amounting to  $0.3\pi$ . (b) Phase shift from the actuation of 4-8 V. This was the only range where an actual phase shift was observable from the data. It generally follows the behavior we expect, where the effects ramps up towards the higher voltages, due to the response going as  $V^2$ . However the result is lackluster in terms of the amount of phase shift. The phase shift is doubled in this case due to the mirror in the end of the device.

interested in finding a device primarily doing  $\theta$  rotations.

A solution to this was to intentionally design the devices  $30[nm]$  larger than the desired outcome after fabrication. With this method we were able to obtain the sizes that were initially intended.

In section 2.2 it was mentioned that a device with broader waveguides should lead to smaller asymmetries in the effective refractive indices of the waveguides, thus constituting a lower amount of phase shift. In turn there will generally be a lower amount coupling between the waveguides as the overlap integral of the evanescent modes and the other waveguide in the vicinity will be smaller. It was however furthermore seen from the analysis of the geometry of these new devices, that the resulting gaps  $d_0$  were smaller in this configuration where the waveguides are broadened in the design process. This will provide a larger coupling as the waveguides are now closer. By examining the results of the full rotation on these type of devices it is evident that a larger change in the  $\theta$  corresponding to the switching capabilities is obtained, combined with a lower  $\phi$  corresponding to the phase shift capabilities. These results are shown in figure 3.14. The resulting range from 0V to 8V which were reached in both parameters was found to be  $\phi(V) \in [0, 0.39\pi]$  and  $\theta(V) \in [0, 1.61\pi]$ . The corresponding Bloch sphere rotation is seen in figure 3.15. It is evident from this that when actuating from 0V to 6V a full  $\theta$  switching is possible

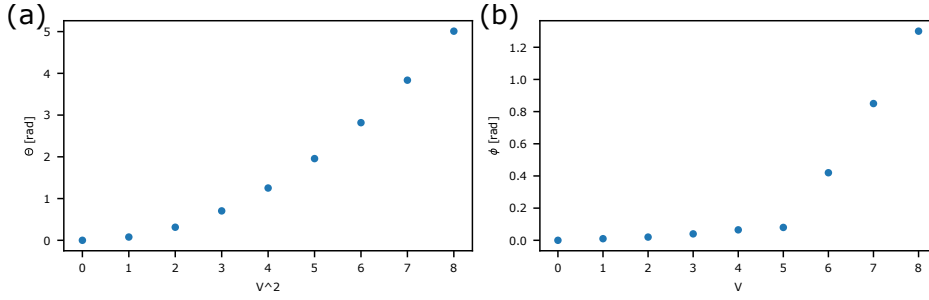


Figure 3.14:  $\theta$  and  $\phi$  for width optimized devices with regard to the switching capabilities: (a):  $\theta$  rotation on the Bloch sphere with actuation between 0 and 8V (b)  $\phi$  rotation with actuation between 0 and 8 V

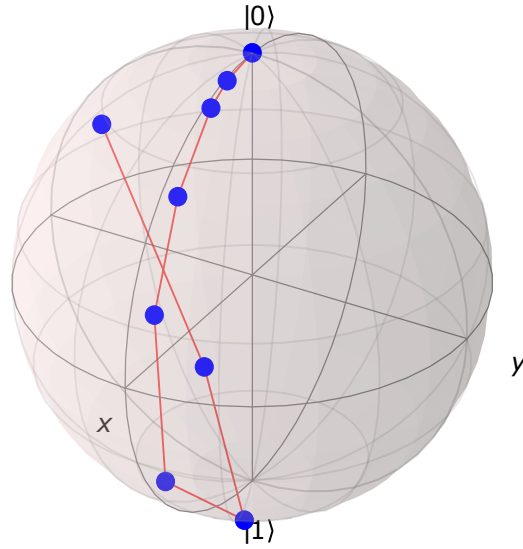


Figure 3.15: **The resulting rotation on the Bloch sphere from a single width optimized operating between 0 and 8V:** The resulting rotation on the Bloch sphere when operating between 0 and 8 V for a single 2x2 device with broader waveguides. Here it is evident that the phase rotation  $\phi$  is much lower than on the narrower waveguides. Furthermore the  $\theta$  rotation is larger. When only actuating between 0 and 6V, a full  $\theta$  rotation is impeded with only a small change in the phase between the arms

with only a small phase change  $\phi$  attributed. This might be sufficient, in addition to the narrower device which was capable of doing a full phase rotation, in order to perform any 2x2 unitary.

### 3.5 Full 2x2 operation

As was seen from the studies of the symmetrically pumped phase shifter the results were lacking in terms of the performance, however it is still interesting to study the effect of 2 independent actuators acting on different independent devices in the same circuit. Control multiple electrically separated NOEMS structures in the same device is a strict requirement for upscaling. This analysis does prove that we are able to isolate the electrical responses well enough in order to have no cross talk between the actuators. There are however still problems that needs to be solved in this regard. When scaling up the system the

complexity of the trenches and the wiring between the different bonding paths increases. As we are yet to have a solution that allows for wires to cross we are limited with regards to how the system can be scaled. In the results presented during this work 4 individual bonding paths were required for a system consisting of 2 independently driven NOEMS devices within the same system. Already a novel approach in the design is required when comparing to that of the usual single NOEMS devices only requiring 2 bonding paths for the electrical actuation of the system. The complexity arises as we require the different electrical components constituting the device to be isolated from each other. The design that was proposed and tested allows for a single qubit operation, given that the devices are capable of sufficiently rotating the qubit on the Bloch sphere, however the exact system analyzed here did not provide a sufficient  $\phi$ -rotation.

Firstly when testing the device we ensured that there was coupling through all the different ports, and that both NOEMS structures could be actuated. The port situated after the symmetrically based phase shifter proved to have a low out coupling, likely due to the MMI's in the system being lossy compared to straight waveguides. We were however still able to get a response that could be analyzed to find the applied phase shift. First the beamsplitting ratio was tested. Here the usual setup is used, by pumping the device and then simply measuring the corresponding output in the arm without the NOEMS based phaseshifter.

The first thing we are interested in however is to observe if there are any unwanted effects arising from the phase shifter. Thus we simply observe the output power from the phase shifting arm with a ramp actuation signal. Here there seemed to be some amount of cavity effects as the amplitude of the corresponding electro-optical signal changes with the voltage. by evaluating the ratio between the maximum and the minimum, as a mean of 40 datapoints near 0V and 7V respectively, it is found that there is a 30% discrepancy between the results, the effect can be seen in figure 3.16. This is however with a large uncertainty associated as the noise constitutes around 10 – 20% of the signal, however it is important to note that these effects are unwanted as the sole purpose is phaseshifting. This will be necessary to analyze in greater depth when analyzing the  $\phi$  rotation obtained from the phase shifter. Here there are results in the range from 2V to 7V, with increments of 1V. This is analyzed in the same vein as the phase shift in the asymmetric case where a fast tukey drive is used between 0 and the desired voltage. Thus enabling us to estimate whether the maximum of the compared sinusoidal fits are varying at different voltages.

For the phase shift measurements themselves in the 2x2 setup, a similar method to previous phase shift measurements is used, this is schematically shown in figure 3.17.b. Here we change the input and output ports, such that input is through the arm with the phase shifter. Outside the setup the piezo is used, to get the setup corresponding to an interferometer with a double phase shift included. Again this will correspond to a shift in the phase of the sinusoidal waves that are fitted, which ultimately gives the phase shift induced by this arm. The result can be found in figure 3.18. Here it can be seen that only a small phase shift of 0.16 rad were obtainable.

For the measurements on the beamsplitting part of the setup constituting the  $\theta$  rotation (which will likely also produce an unwanted phase shift in  $\phi$  due to the fabrication asymmetries that are created in the structures) the same method as the single devices is used, with the schematics of the experiment being shown in figure 3.17.a. Here we simply utilize the port without the phase shifter as the output port in order to obtain the best signal to noise ratio, this will allow for determination of the splitting ratio and associated phase shift. These results are presented in figure 3.19

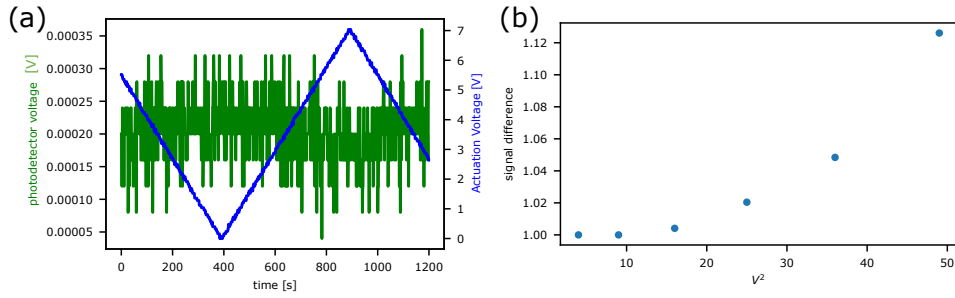


Figure 3.16: **Cavity effects in phase shifter:** (a) A ramp signal (blue) is send over the MEMS in the phase shifting arm of the  $2 \times 2$  unitary build. From the photoelectric response (green) it is observed that there is a slight change in the amplitude of the signal at different voltages. The signal to noise ratio is however not great. (b) the ratio between the maximum at 0V compared to the maximum at the given actuation voltage squared. Here a clear connection between the actuation voltage and the intensity measured can be seen.

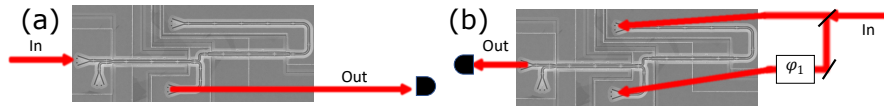


Figure 3.17: **Experimental sketch of the  $2 \times 2$  unitary measurements:**(a) Method used for the initial beamsplitter/phaseshifter (b) experimental setup used for the symmetrical phase shifter, in the form of an interferometer with 2 phases

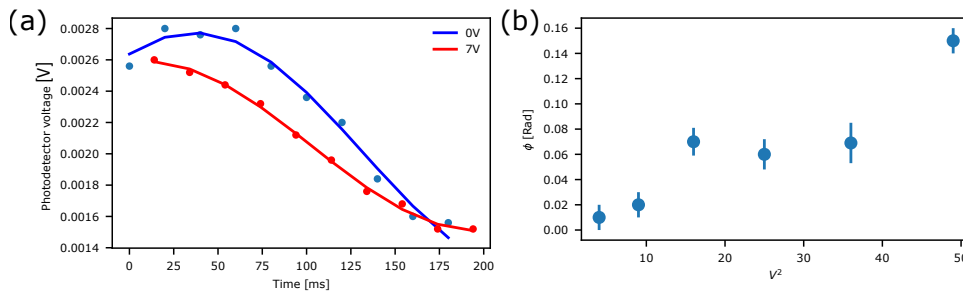


Figure 3.18: **Results of the symmetrically based phase shifter in the  $2 \times 2$  setup:**(a) For to the 0-7V actuation. Here it is evident that there is some intensity modulation as well as the phase shift (b) Result from all fits between 2 and 7V. At voltages below this no effect was seen.

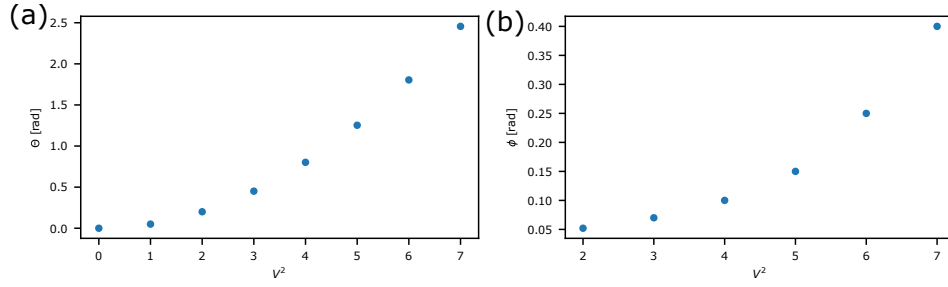


Figure 3.19: **Results of the Beamsplitter NOEMS in the 2x2 unitary:**(a) The beamsplitting phase  $\theta$  induced by the beamsplitter from 0-7V (b) The phase shift between the 2 arms  $\phi_{BS}$  induced by the beamsplitting part of the 2x2 circuit

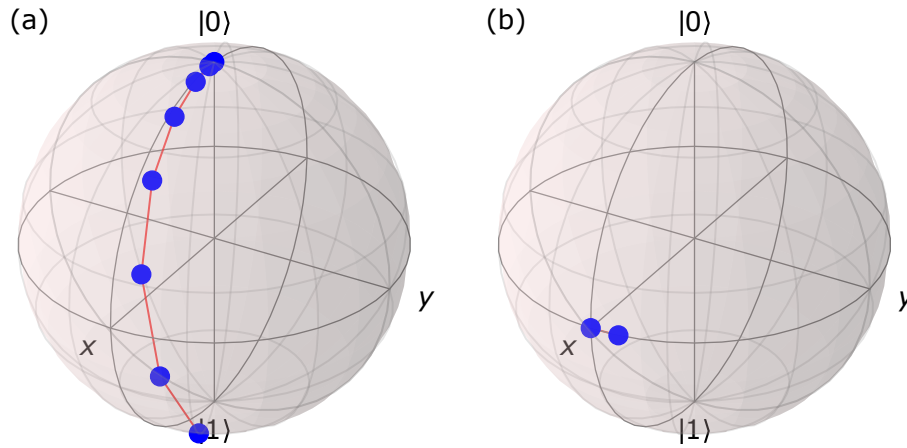


Figure 3.20: **All rotations available on the Bloch sphere in the 2x2 unitary where both devices can be actuated from 0 to 7V:**(a) The  $\theta$  and  $\phi$  rotations induced by the beamsplitter, here the  $\theta$  rotation is sufficient, and the unwanted associated  $\phi$  rotation is almost negligible. (b) the  $\phi$  rotation imparted by the symmetrically based NOEMS device. Here only two points corresponding to 0 and 7V are shown for clarity purposes. It is evident that this rotation is far from the desired full  $2\pi$  rotation

Finally this allows for the reconstruction of the 2 different rotations on the Bloch sphere that are independently available via the actuation of the 2 NOEMS devices in the circuit. Here the result is shown in figure 3.20. Noteworthy the beamsplitting part of the device gives more symmetrical results with a lower amount of phase shift  $\phi_{BS}$  from this part, while still being able to almost complete a full  $\theta$ -rotation

It is clear that the beamsplitter is sufficient, and that it has been an improvement to make the waveguides wider in order to lower unwanted phase rotations due to fabrication limitations. This agrees with the complete Bloch sphere rotation found from the improved beam splitter. This did however also come with the cost of a generally lower beamsplitting range, nevertheless better splitting ratios with the same NOEMS design has been shown for the single devices. As of now the problem primarily arises in the phase change, it is a novelty that both of these operations can be done independently, which is a promising result even with the lacking  $\phi$  rotation. It seems that the fabrication limitations in general is an issue for designing symmetrical structures which is highly needed in order to obtain a useful phase change with this method, thus another device needs to be implemented in

the setup in its place. If a NOEMS based phase shifter is somehow realized however, it can be directly inserted in the geometry shown here in order to perform any arbitrary 2x2 unitary rotation on the Bloch sphere.

### 3.6 Mechanical Properties

On top of the different optical operations that can be done, it is necessary to investigate the mechanical properties of the system. These will be the limiting factors in terms of switching speeds, and the precision of the intended operations.

The maximal speed of the operations are limited by the mechanical resonance frequencies in the system. As the system consists of 3 cascaded directional couplers, where there might be asymmetries between the waveguides, it is expected that we can observe multiple resonance frequency for each of the modes. Furthermore the lowest resonant modes are those that are moving opposite to each other, giving large optical responses. Thus if these are excited, a rapidly oscillating signal will be seen optically at the output ports, probably even if we are only actuating the mode with the lowest resonance frequency. The relaxation time when oscillations are introduced is dependent on the Q factor, which is inversely proportional to the line-widths of the frequency peaks. A larger Q-factor will imply that the oscillations will continue for longer time periods before reaching an equilibrium position. As we are concerned about switching speeds, which will be of importance when doing single photon experiments with the system, it is of interest to operate in a region where these modes are not excited, as the relaxation times are much longer than the time it takes to actuate the system below the resonant frequencies. Thus a study of the resonances are conducted, this is done by sending a noise signal as the actuation over the NOEMS, hereby a Power spectral density (PSD) measurement can be conducted as described in section 2.5. The resulting resonance frequencies of the system can be seen as peaks in the frequency spectrum of the applied noise. This is seen in figure 3.21 and 3.22.

Here it is evident that the lowest order modes, with the lowest resonance frequencies are situated at  $\approx 1.3MHz$ . The fastest switching time is inversely proportional to this value seemingly leading to the conclusion that we are restricted to do operations slower than  $\approx 0.7\mu s$ . A curious result is that we are not seeing a mode from each of the cascaded parts of the device.

Furthermore an analysis on the first set of devices was done, to estimate the relation between the device length, the resonant frequencies and the Q factors. For this all the functional devices on the chip was analyzed with the aforementioned PSD method. Afterwards the resonant modes for the lowest order modes was determined by fitting lorentzians to the corresponding data. As the initial gap  $d_0$  should have no influence on the mechanical properties of the individual waveguides, we can bunch together devices of similar lengths to obtain larger statistics for this analysis. Note however that different devices might have slightly varying widths even though they are designed with identical properties, this leads to fluctuations in the resonance frequencies. From figure 3.23 we can see the expected behavior, that the mechanical resonance frequency follows of  $f_0 \propto L^2$  where all other geometrical parameters are kept constant.

The limiting factors determining the mechanical resonance frequencies of the waveguides are primarily related to the size of the waveguides. A larger waveguide, both in terms of length and the transverse width, will have a lower resonance frequency. A couple of different solutions might be possible if we intend to make the system faster. One

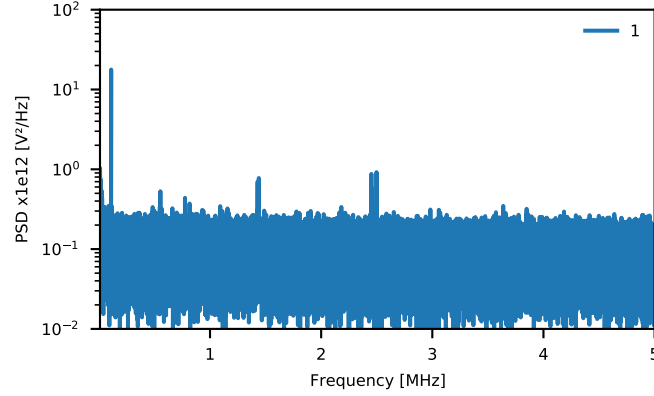


Figure 3.21: **PSD scan of the first type of device with no cascaded devices:** Full PSD scan between 0 and 5 MHz for the first type of device that was analyzed. This was mainly to get an idea of the modes for the individual waveguides in the system. The modes show as Lorentzian peaks in the spectrum. Artifacts from the laser and detectors will show as sharp peaks without the Lorentzian behaviour.

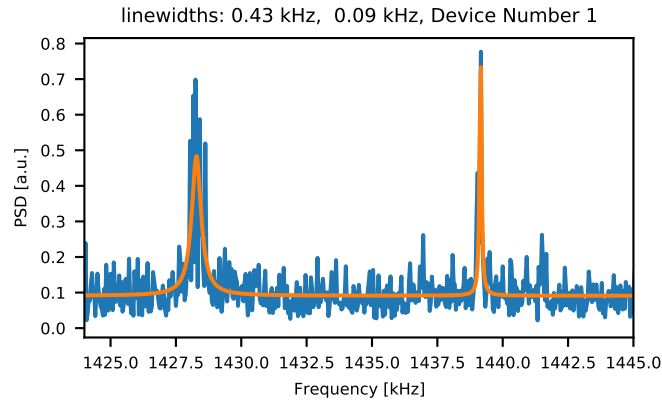


Figure 3.22: **Example of fits to the 2 peaks arising from the asymmetry in the waveguides:** For this type of device 2 Lorentzians are always seen close to each other, corresponding to the same resonant modes in the 2 waveguides with asymmetry in the widths. The linewidths are listed, this is used to evaluate the  $Q$  factor which is inversely proportional to the linewidths.

solution would be to use a larger number of cascaded devices, where in turn each of the cascaded sections are shorter. The setbacks from such a solution would however a longer total footprint of the device, as more tethers are needed between the different sections. The geometry of the waveguides are at the lower limit of what is tolerable with regards to losses. The fabricated and tested devices had waveguide widths of  $\approx 190 - 200$  nm. From earlier studies it is known that narrower waveguides will suffer intolerable losses. Another solution would be to decrease the gap between the waveguides. From simulations it is evident that the prospects of working in the regime below a gap of 100 nm are promising. This could lower the length of the devices, while still retaining the capabilities of full switching in both parameters. All of the aforementioned solutions will however only increase the resonance frequency with a factor of  $\approx 2$  realistically.

When testing the limits of the fastest possible switching time, it is necessary to use a well tailored function for the actuation signal. As mentioned previously and shown in



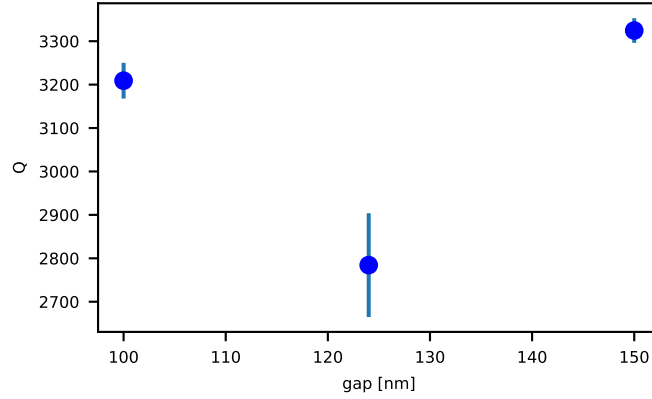


Figure 3.25: **Q Factor as a function of the varying gap between devices:** All Q factors for the varying gap sized with the same waveguide widths. There seems to be no clear correlation between waveguide widths and the Q factors which was the expected result.

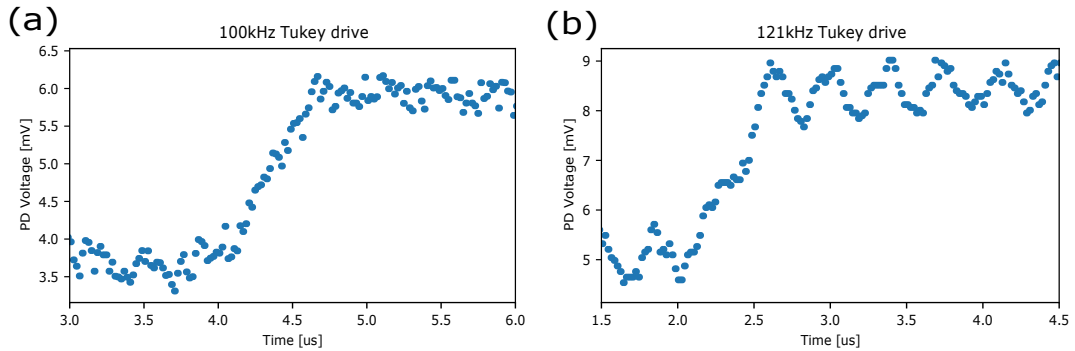


Figure 3.26: **Different Tukeys signals applied to find the maximal switching speed:**(a) an example of the fastest possible switching speed without inducing oscillations in the system. the 10-90 rise time is  $\approx 650ns$  (b) a slightly faster switching which introduces oscillations. It is obvious that the time it takes for the oscillations to dampen is far greater than the time it takes to actuate slower.

### 3.7 Noise measurements

When estimating the noise and sensitivity of the structures it is important to note that these values will depend on the setting of the structures. In order to estimate the noise we calibrate the devices in order to find the setting with maximal noise levels. An example of the calibration can be seen in figure 3.27. The aim is to find the voltage setting for each of the devices where the splitting ratio is  $\approx 50/50$ . This is the region where the slope of the output signal with respect to the changing voltage, and thus the change in the gap, is largest. Thus this will be the most noisy area, meaning the largest response in the frequency spectrum of the PSD will be found here. This was tested in depth for a single device, where all the voltage steps was applied and the spectrum was analyzed. The largest response was found in the expected area with a 50/50 splitting ratio as expected. This will thus be the point where noise is estimated. Noteworthy the calibration measurement (blue) in figure 3.17 is carried out individually for all devices, as the responses are different. Hereby the 50/50 splitting response can be found for each device in order to observe individual noise responses.

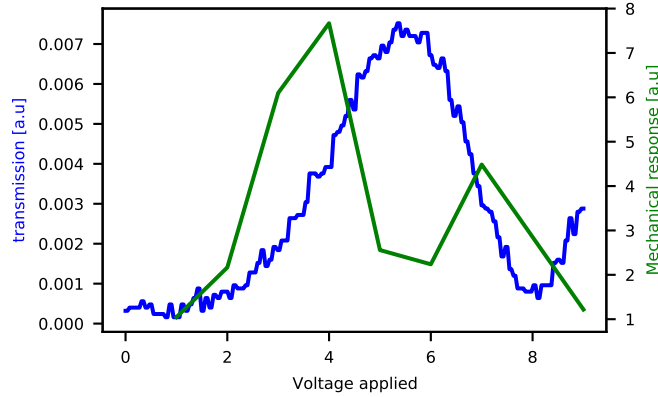


Figure 3.27: **Sensitivity calibration and measurement:** A ramp between 0V and 9 V is applied, the corresponding output photons in the transmission channel is measured. Afterwards a sensitivity measurement is done at each voltage with a step of 1V. The sensitivity measurements show the predicted outcome, that the noise ratio and thus the amplitude of the mechanical mode has the largest optical response at the 50/50 splitting intervals, and the lowest response where the derivative of the transmission curve is zero.

When completing the calibration and noise measurement for the maximal noise in the device some curious responses were found. In some devices no clear resonance peaks were found, even though we confirmed that the devices were indeed still active. This could lead to the conclusion that some of the devices are indeed very stable in terms of oscillations at a set DC voltage. Thus when dialing a certain combination of  $\theta$  and  $\phi$  as all devices will produce a rotation in both phases, these values will be very stable.

Another interesting property of the mechanical responses at different voltages is the change in resonance frequency vs the applied DC voltage. It seems that there will be a linear relation between the  $f_{res}^2$  and  $V^2$ , at least until the displacement start to become noticeable at larger applied voltages. This is an interesting effect in and on itself, it might however also be directly applicable and useful towards resonantly driving the system. If we want to utilize the resonant driving of the devices, which will greatly increase the achievable switching speeds, it is necessary to have devices responding to the same resonance frequencies. As all waveguides designed are slightly different due to fabrication limitations and errors, they will have different mechanical responses. Thus it will be unlikely that 2 separately fabricated devices will have the same response. By applying a DC current over the sample we can however bring the frequencies to match, as long as they are within the frequency tuning range of each other. The tuning range of device 1 can be seen in figure 3.31 where the resonance frequencies as a function of the applied voltage is plotted.

Thus if the mechanical resonance frequencies are within  $\approx 0.05[MHz]$  it seems possible to match resonances by simply applying an external DC voltage on top of the AC signal.

### 3.8 Resonant driving

We are interested in investigating the effects of resonant driving beyond what has previously been studied. This is done by applying an AC current over the sample. We chose a current on the form  $V = 1 + \cos(\omega t)$ . The additional 1 is necessary as there for some reason is no response for negative voltages in the system. The response from the NOEMS will follow  $V^2$  thus this will be on the form  $1 + \cos^2(\omega t) + 2\cos(\omega t)$ . From the mode

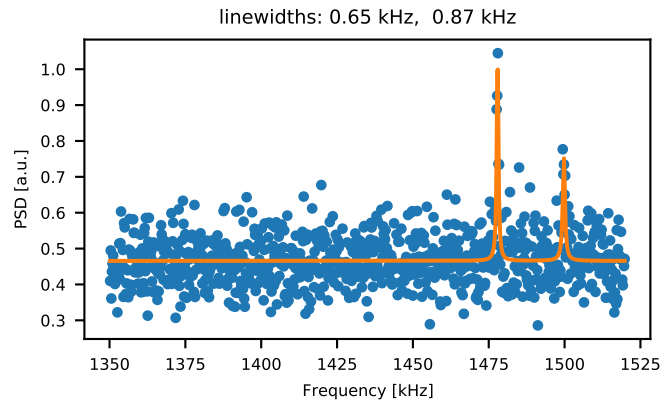


Figure 3.28: **Noise measurement of device 1:** Minimal response in the frequency spectrum of device 1. This was found at 1V. Curiously even though the device consists of 3 separately cascaded parts only 2 resonances show up for each of the modes, corresponding to the 2 parallel sections that has slightly varying widths

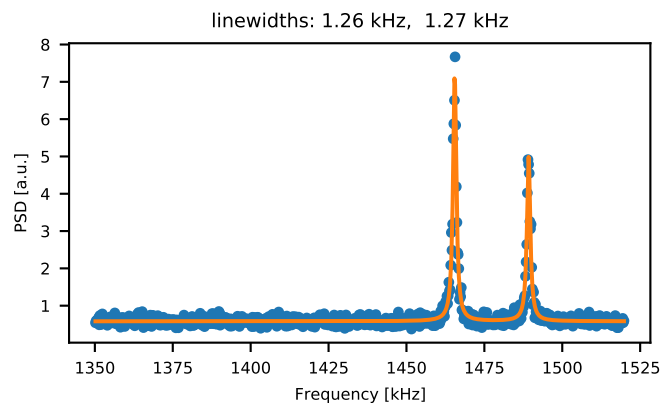


Figure 3.29: **Maximal response of device 1:** The maximal response for device 1 was found at 4V, here the splitting ratio is  $\approx 50/50$  as we expected. Here the resonances are much clearer and the linewidths along with the actual resonance frequency is better determined.

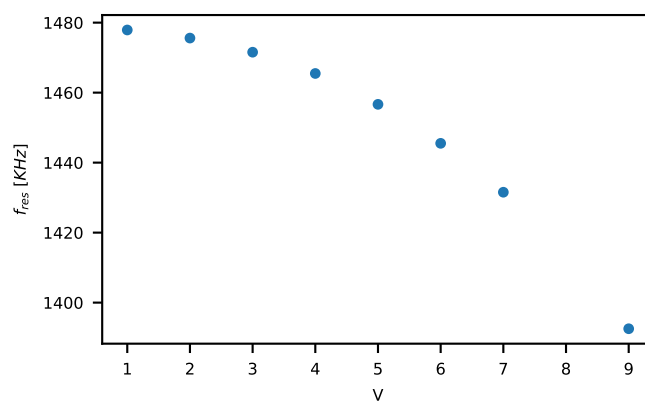


Figure 3.30: **lowest order resonance frequency of one waveguide with respect to the voltage applied:** The change in resonance frequency as a function of the applied DC voltage. It is clear that for this particular device the tuning range is in the order of  $\approx 0.1[MHz]$

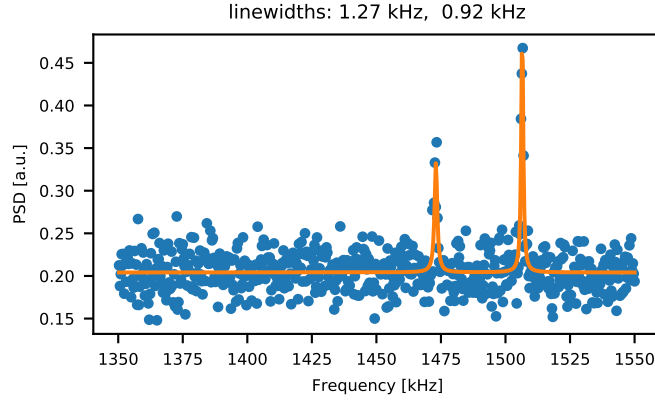


Figure 3.31: **Resonance frequency at the 50/50 ratio for device 6:** The resonance frequency of device 6 at the point of maximal sensitivity. This occurs at 2.9V. It is clear that this frequency is within the tuning range of device 1. This means that we would be able to set a DC signal over these devices which will bring them to similar resonance frequencies. This show the possibility of driving different devices resonantly in a circuit at the same frequency, possibly allowing for different demultiplexing schemes.

analysis of the different devices, we know the responding frequencies. Furthermore it is known that there are at least a couple of different resonances which are optically active in the systems. These are from the different modes in the 2 distinct parallel waveguides. Furthermore it is known from section 2.5, that the responding amplitude is dependent on the Q factor of the resonant mode that is excited. We thus vary the frequency of the applied AC signal in order to reach the different resonances and observe the effect on the splitting ratio. Previous studies of similar systems dealt with the response of the first order resonance [7], however if other modes are also capable of doing a full switch it is likely more interesting to investigate those as these will be switching at faster rates due to greater resonance frequencies.

Interestingly when scanning the frequency range, we found differences from the PSD analysis. Specifically we found a resonance for device 11 at a frequency of 2.36MHz, seen in figure 3.34. As we also saw no peaks for this device when doing the sensitivity measurements, and with the knowledge that this device can actually be actuated and thus its not broken, it seems that the levels of noise are indeed very low, and that we are able to actuate resonant modes that does not show clearly in the spectrum analysis. This complicates the procedure a bit, as the Q factors are generally of interest in order to know how strongly we can drive the resonant modes without breaking the devices. An estimation of this factor is not possible without any resonance peaks. Another interesting property of this exact mode is that it has a larger switching ratio than the lower order modes. This mode is even capable of doing a  $\theta > \pi$  rotation for the splitting ratio, meaning that more than full switching is possible. Furthermore this even increases the speed in which this switching can be done, as it switches completely in about half a period compared to the applied signal. All the possible resonant drivings that were observed are shown in figure 3.32-3.34.

It is however complicated to determine whether it is actually switching completely from the minimum to maximum output in the transmission/reflection ports. This is due to the fact that the photo detectors in use has a greater response at larger frequencies. Thus the output signal when switching with the resonant driving is larger than for a ramp

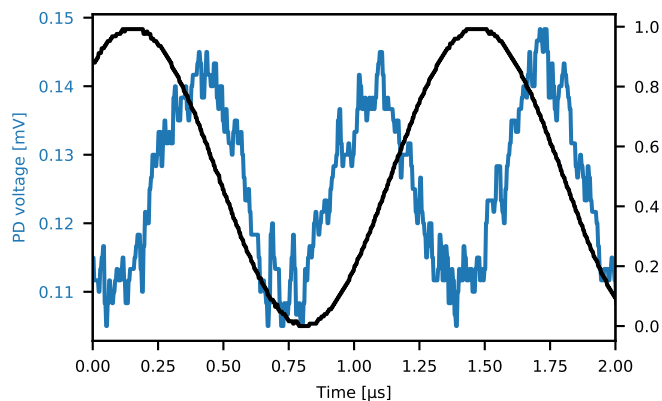


Figure 3.32: **Resonant driving at 1.33 MHz:** Resonant driving of the lowest order resonance frequency. Here the switching time is  $\approx 0.25[\mu s]$

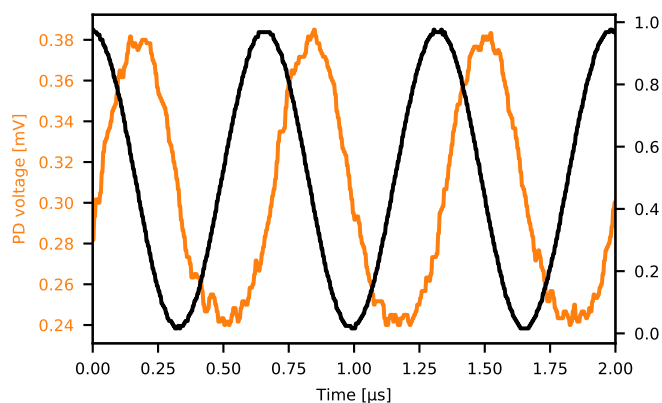


Figure 3.33: **Resonant driving larger frequency:** Resonant driving of the second lowest resonant that was found. Here the switching time is  $\approx 0.25[\mu s]$

signal used for calibration. One thing that can be said from this however, is that the off-switching level is similar in the 2 cases, meaning that we can conclude that almost no light is transmitted at this setting.

### 3.9 Phase stability

One important aspect is to be able to do the desired rotations on the Bloch sphere on demand, another is the speed at which it can be done and finally we need to ensure that the rotations are stable, in the sense that there is no instability in the phase (either  $\phi$  or  $\theta$ ) once these has been set in order to ensure that we are actually doing the intended operation. These effects might be due to different phenonemons, one of which has been discussed earlier is the optomechanical response, where the force from the light source affects the position of the waveguides. It was however seen that the optomechanical effects were quite low in most structures, and that it was even difficult to find the mechanical resonance peaks that could lead to instabilities in the phases. Another effect, which is likely to be the dominant effect are thermal effects causing movement in the setup. Throughout this project we only experimented at room temperature, these effects can be directly transferred to the cases of single photons, however in this case the temperature dependent fluctuations should be much lower as a requirement for these experiments is

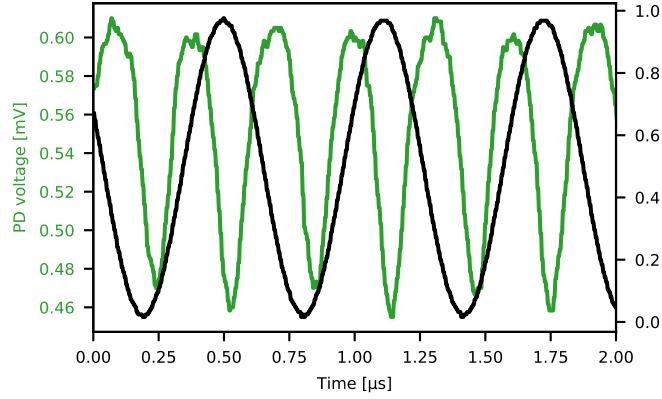


Figure 3.34: **Resonant driving**: Resonant driving an even larger order mode. Here the switching time is  $\approx 0.1[\mu s]$

cryogenic temperatures. It is still interesting to analyze the effects at room temperature as this will at least serve as a reference on the maximal amount of noise we can expect. Other effects such as the opto-mechanical motion and Q factors of these resonances will likely be increased in the case at cryogenic temperatures. We do however expect the thermal effect at room temperature to still set an upper limit.

In general a varying amount of phase instability will be present, depending on the setting of the phase shifter/beamsplitter. This will in general depend on the derivative of the response signal, meaning that in the case of the  $\cos^2(\theta)$  response of the beamsplitter this will be maximal at the 50/50 setting where the largest derivative is found. Furthermore the lowest amount of phase noise will occur at the 100/0 splitting ratios as the derivative is essentially 0 in this point, meaning that a bit of fluctuation in the position of the waveguides will not affect the optical response. In order to estimate the phase noise we chose to operate at the point of maximal transduction, specifically the voltage with a 50/50 splitting ratio as we are mainly interested in setting the upper limit for the expected noise. This calibration is seen in figure 3.35.a here a full voltage scan is performed to cover the entire switching range. Evidently at around  $V^2 \approx 40$  the splitting is 50/50 in the output ports, this is thus the position where we park the device in order to do the PSD measurement used in figure 3.33.b where the maximal phase instability is found.

Here a PSD measurement is done over all frequencies of the device. All frequencies are integrated, both for the signal itself and the corresponding background noise which stems from the laser. Such that

$$\delta\theta = \int s(f)df - \int s_n(f)df = 0.0037rad \quad (3.3)$$

This result has mean that the variance is similar to that of current state of the art thermal phase shifters, which is  $10^{-5}$ [9]. Noteworthy is that this is the case at room temperature. Thus we expect lower noise levels when operating at the single photon temperatures of  $\approx 4K$ . Our hypothesis is that the phase noise is inversely proportional to the temperature thus we can estimate how it will change for lower temperatures. In the future similar devices will be operated at  $\approx 4K$  to support single photons. A crude approximation is that the noise level is inversely proportional to the temperature. Thus, if the hypothesis is true, when going to the cryogenic temperatures its supposed that the phase noise ends up far superior to the case of thermal phase shifters. This does however need to be proved

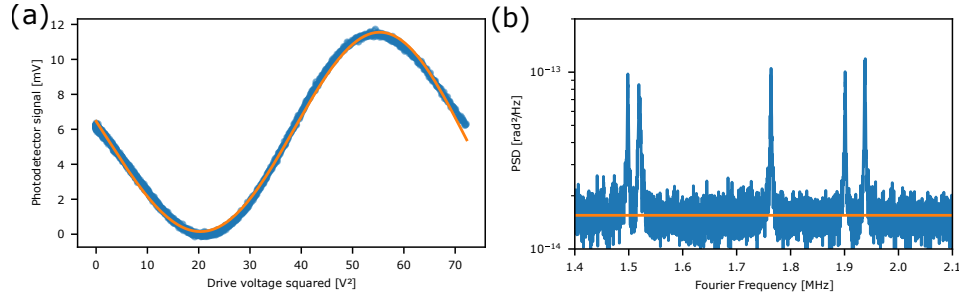


Figure 3.35: **Phase instability:** (a) Full switching here the  $\theta$  can be tuned between 0 and  $2\pi$ , the points of the maximal transduction is when the splitting ratio is 50/50, around  $V^2 = 40$  (b) Spectrum at the point of maximum transduction (blue) and the background light noise (orange), here the light noise is subtracted and the rest is integrated giving a phase noise of  $6.5\mu\text{rad}$  at a temperature of 300 K

experimentally.

The phase stability plays a critical role when upscaling the system as there will generally be a limit on the amount of noise that can be tolerated under these circumstances while still having a functional network. This is described in section 2.5 via the n-bit precision. Here it was demonstrated that errors in the range of mrad's was sufficient for large up scaling of the system while still keeping a n=10 bit precision. Thus if the devices are indeed capable of reaching lower limits they will be very compatible with larger networks.

### 3.10 MMI response

In order to get a better understanding of some of the effects induced by the MMI in the system, this includes losses and possible side effects at different wavelengths. In order to do this, structures with 2 MMI's was compared to a similar structure with straight waveguides. This was done by the use of the super-K laser (a supercontinuum laser) Where the wavelengths are in the range between 900-1050 nm

The analysis show that the MMI structures are quite lossy, as 2 subsequent MMI's give approximately 40% of the output light compared to the straight waveguides. It would thus be beneficial to optimize the transmission in the structure if these are utilized in the future. However it is often the case with on chip beamsplitters that these will induce a much larger amount of losses, meaning that the symmetrical pumping phase shifter is likely not suitable for upscaling, even if the phase shift induced were satisfactory. Furthermore there seem to be no extra cavity effects or extra reflections in the MMI's at different wavelengths compared to the straight waveguides as can be seen in figure 3.36.c, here we see that they both have the same fringes, likely these are from the super-K laser itself.

It would have been interesting to analyze which splitting ratios the MMI's are producing. This would help with a better understanding about the limitations in the symmetrically based phase shifter. It is certain that something is different in the fabricated structures compared to the ones simulated in COMSOL as the phase shifts are lackluster. It would be of interest to understand how much of this effect is due to an unwanted splitting ratio from the MMI, and how much is due to the fabrication limitations in the symmetry of the waveguides. From earlier analysis it seems likely that the asymmetry

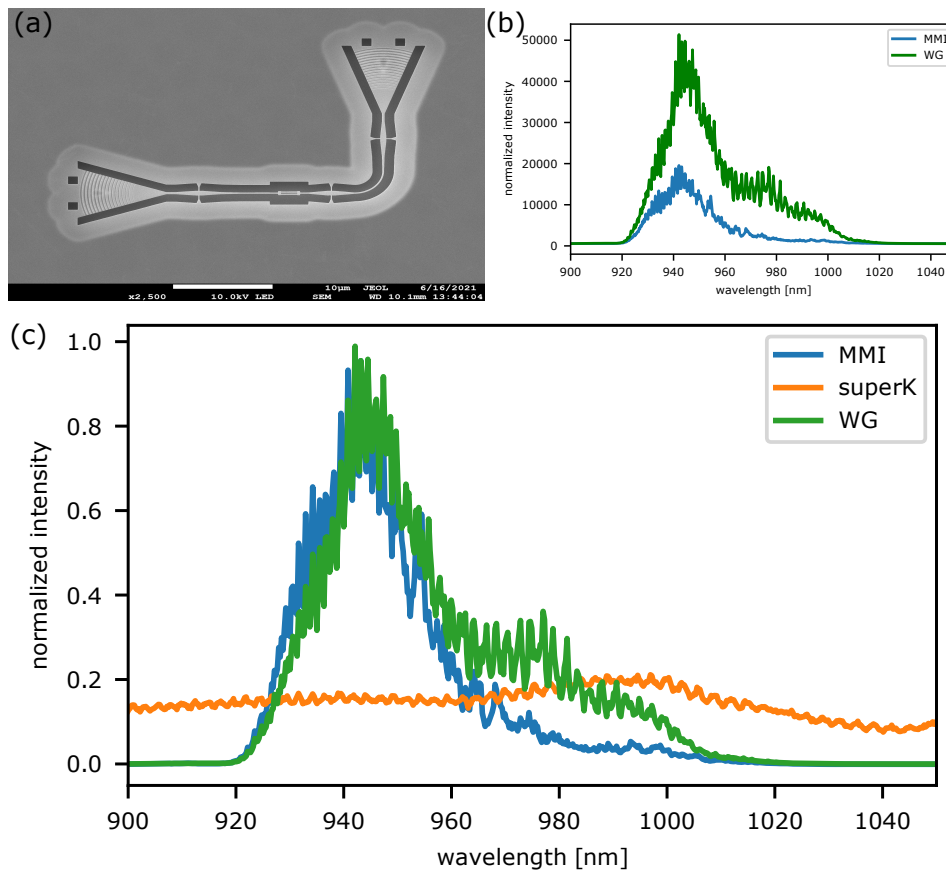


Figure 3.36: **Analysis of MMI response:** (a) Straight waveguide structure with MMI's. The compared structure is alike simply without the MMI's (b) The power measured through the MMI waveguides (blues) and the Straight waveguides (green). It is evident that the power is  $\approx 40\%$  when going through 2 MMI's (c) normalized spectrum with the inclusion of the super-K spectrum. Here it can be seen that there are both fringes in the MMI response and the straight waveguide response, which matches the fringes induced from the super-K. Thus there should be no extra cavity effects arising from the use of the MMI's.

arising from fabrication is a problem that will always arise with the current fabrication technology, thus if this is the main source of error the symmetrical phase shifter can be ruled out as a viable option, as we will never reach a sufficient amount of symmetry in the structures. However if the problem primarily arises from the MMI's in the design, then this might be a solvable problem where a phase shift closer to  $2\pi$  might be obtained. The other limitation as has previously been mentioned is the losses arising from the use of an MMI (and likely also other on chip beamsplitters). Thus inquiring an unbalanced amount of losses in each of the  $2 \times 2$  unitaries, thus impacting the up scaling capabilities greatly.

## Part IV

# Discussion and outlook

# Chapter 4

## Outlook

Throughout this thesis promising results has been shown towards using the NOEMS devices as both a phase shifter and beamsplitter simultaneously. It has been demonstrated that it is possible to construct a device capable of doing a full  $2\pi$  rotation in  $\phi$  on the Bloch sphere at as low as 7 V's of actuation in devices shown in section 3.1. These types of devices furthermore has a low amount of phase instability with a variance of  $\approx 10^{-5}$  rad at room temperature, it is hypothesized that the variance will be even lower at cryogenic temperatures. Furthermore similar devices with broader waveguides are capable of producing a full switching between the output ports meaning a full  $\theta$  rotation, while only contributing with a small amount of phase shift, the  $\phi$  rotation. These results are shown in section 3.4. This, combined with the ability to independently actuate 2 separate NOEMS devices might be used towards making any 2x2 unitary in the future as shown in section 3.5. However, in order to scale to larger operations new methods of wiring and bonding the devices are necessary. Furthermore it has been demonstrated that a phase shift based solely on the symmetrical pumping of the NOEMS devices is possible. However the results obtained from this was rather lackluster as only a small change of 0.3 rad in  $\phi$  could be produced. It seems that current fabrication limitations are an issue towards realizing a fully operational phase change with this method as asymmetries will seemingly always arise in the fabrication process of the structures. It was however demonstrated that these devices could be tested by using an on chip interferometer, thus not requiring sophisticated external experimental setups.

A thorough analysis on the mechanical properties of the devices was also carried out, showing the relations between properties of the mechanical modes in the system and the NOEMS geometries, including resonance frequencies and quality factors along with the instability of optical settings of the devices. Finally the prospects of resonant driving was also investigated, it was shown that great switching speeds were attainable by driving higher order resonant modes of the NOEMS devices, however to much confusion the resonant driving required much larger driving voltages than initially anticipated. As the devices that were analyzed was the new cascaded version of the NOEMS devices, the exact properties of new and complicated modes needs to be analyzed further in order to completely understand the prospects of driving the devices resonantly towards the use in demultiplexing schemes. It was however demonstrated that the resonance frequencies of the devices can be tuned by applying a static voltage over the devices. Several devices were analyzed this way and it was proven that some of the devices were within a range where they could be tuned to the same resonance frequencies. This is crucial if the resonant driving is to be used in the future. As the resonant modes are dependent on the exact geometry after fabrication, and as there proved to be limitations on this, it is not likely that 2 devices designed with the same properties will have the exact same resonance

frequencies. However if they are simply in close proximity we are able to set them in resonance with each other.

There are however multiple challenges that needs to be overcome in order to obtain the ultimate goal of producing any  $N \times N$  unitary, or having a NOEMS device that works solely as a phase shifter. First and foremost while a phase shift of  $2\pi$  in  $\phi$  has been shown with these devices, they are based on the asymmetric design which also leaves us with a change in the splitting ratio  $\theta$  when actuating the devices. It was seemingly possible to construct a device with more symmetrical properties by making the waveguides broader, thus lowering the amount of  $\Delta n_{eff}$  between the waveguides. This did however still come with a small phase shift, which would lead to uncertainties in the settings of a future  $2 \times 2$  device based on the 2 aforementioned devices. The aim for future developments is thus to construct a device with as symmetrical features as possible, in connection with the asymmetric device, since as long as the full phase shift can be produced, a device capable of producing the full rotation in the  $\theta$  regime will be sufficient in order to put the output state on any point on the Bloch sphere.

The limitations are however that the 2 operations are not done independently, thus extra considerations needs to be taken into account when trying to achieve the full Bloch sphere rotation where 2 devices are needed. This problem would readily be solved by with the realization of a symmetrically pumped phase shifter only acting on one of the arms. This work was not able to produce such a device, nevertheless it does seem possible given the results from simulations. Thus if the fabrication issues are solved, and the devices that can actually be produced are closer to the intended design, the effects from such a device should be feasible to obtain experimentally as well. With such device the full Bloch sphere rotation can be implemented with existing NOEMS devices and ready for testing. If the production of such a device is not a possibility, it should still be possible to switch basis in which the rotations on the Bloch sphere are done, where the phase-splitters are now used with 2 subsequent devices as explained in section 3.2

Another current limitation of the system is related to the length and speed of operation. This is dependent on the lowest order mechanical resonance frequencies in the system. It was demonstrated in section 2.2, that this is dependent on the geometrical size of the waveguides that are used. Making the waveguides narrower would increase the amplitude of the evanescent fields of the waveguides, thus increasing the amount of light that will couple between the waveguides and effectively decreasing the required length to observe the wanted effects. This solution will however have limitations as the effective refractive index of the waveguides varies rapidly in a more narrow region, thereby surface roughness will impose larger losses in the system. This solution is thus not a feasible solution. Another method would be to cascade the devices a larger number of times, while keeping each of the cascaded parts shorter, thus decreasing the length of each part and increasing the resonance frequencies. This could be a solution to be investigated further, but it will increase the footprint of the devices, and will likely produce larger losses, as each of the tethers are more lossy than the waveguides themselves. Furthermore this is not enough to decrease the switching speeds drastically.

The gap between the waveguides is another effect that could be investigated further, in terms of obtaining greater coupling and decreasing the lengths of the devices. At the moment we are limited in terms of fabrication in a way where devices with gaps smaller than  $\approx 100$  nm. Thus we are already operating at the limit of what can be physically realized. Another way to get larger effects would however be to change the direction of how the waveguides are moving when they are actuated. If possible, larger effects would occur,

when the waveguides are moving towards each other instead of being pulled apart. The limitations with this method is that the waveguides can only go to  $2/3d_0$  where  $d_0$  is the starting position for the waveguides. This is a slightly smaller amount compared to how much the waveguides are approximately moving apart. However the effects become much larger in this region, possibly enough to get even larger effects at shorter coupling lengths  $L_C$ . This does require a new design and architecture for the waveguides and actuation process. This will already have an effect on the mechanical resonance frequencies. On top of this much larger effects are observed, at least in simulations, when the waveguides attracted instead of pulled apart. This can either be utilized to cascade the device fewer times, or to decrease each of the cascaded parts, depending on whether the main interest is to decrease switching speeds or to decrease the total length of the device drastically. The simulated effects of these changes can be seen in figure 2.5, here it is evident that much larger effects than previously observed are occurring when the gap  $d$  decreases below 100 nm.

This method does also have its limitations, it will likely have more losses than the earlier structures, and as it is not a device that has been realized in the laboratories yet it is uncertain how well it will actually perform outside simulations and whether it is even realizable or not.

## Phase rotation

One of the main goals was to construct a device acting solely as a phaseshifter for direct implementation in a 2x2 unitary operation with existing beamsplitting techniques. The method of performing only a  $\phi$ -rotation on the Bloch sphere was attempted with the symmetrical setup. While this is seemingly an elegant solution, and feasible from a simulations perspective the obtained result was merely a phase shift of  $\phi = 0.3\text{rad}$ , thus far from the necessary  $2\pi$ . Solving this would require an enormous up scaling of the number of cascations in the system, while this would have similar switching speeds, as this was shown to be limited primarily by the individually cascaded NOEMS structures, the losses amounting from the vastly increased footprint would not make this solution feasible.

As there are a couple of novelties included in this structure it is not that clear to determine exactly what effects differs so drastically from the simulated example. Firstly an attempt of making an on chip interferometer was done, however for comparison there was also the phaseshifter in the 2x2 unitary and these gave similar responses so the issue should not lie here. Asymmetries and general variations from the intended design arose in all the structures where a sufficient SEM-imaging was performed to determine the properties of the systems. Sufficient data is not available to determine if this was also the case for the symmetrically based phase shifters, however it is of course highly likely that similar effects were seen. This is thus breaking the symmetric mode, which the phaseshift relies on, its not clear how much of an effect this will have on the obtained phaseshift but it might prove to be one of the answers to the difference between the simulated results and the measured results. On top of the NOEMS themselves being symmetrical it was also important to ensure symmetric pumping of the system, an attempt towards this was done with the use of MMI's as explained in section 2.2 and appendix A.2. The optical response of these are nevertheless highly susceptible to geometrical variations, which are probably also occurring here. Thus in conclusion it seems that we are both unable to construct a perfectly symmetrical device, let alone actually pump it symmetrically. It is not clear as of now which of these effects will have the largest impact on the achievable phaseshift, and

this will thus need further analysis.

As the symmetrical approach is seemingly a hurdle towards making a full 2x2 unitary, it seems to suggest that other methods might be favorable. The arising asymmetries in all of the structures did however prove to give the ability of a full  $2\pi$  phaseshift. This seems to be a, perhaps less elegant, but at least feasible way to construct a phaseshifter based on NOEMS structures. One of the limitations here however is the inability to predict the exact amount of asymmetry that arises, from the simulated results in section 2.3 and the study of both narrow and wider waveguide structures, it is evident that the amount of achievable phaseshift is a highly variable property. It is thus still necessary to better understand these effects in order to anticipate the magnitude of the effect.

## Future work

Firstly it would be interesting to do further analysis of the devices at cryogenic temperatures. This is both to ensure that there will still be similar ranges available in  $\theta$  and  $\phi$ , but furthermore in order to investigate how the mechanical responses changes here. The phase noise is hypothesized to decrease dramatically at cryogenic temperatures as the effects are primarily thermal.

Furthermore as all the requirements for doing a full arbitrary rotation on the Bloch sphere, including a  $\theta$  rotation of  $> \pi$  without substantial rotation on  $\phi$  and another independent device capable of doing  $> 2\pi$  rotation in  $\phi$  it seems that a full 2x2 unitary can be constructed. As it has also been demonstrated that doing 2 independent operations is possible these can be combined much in the same manner as the try of doing the full unitary that was shown here. Instead 2 NOEMS will simply be placed in series, one having broader width of the waveguide to do primarily a  $\theta$ -rotation, while the other has narrower waveguides, thus larger relative asymmetry, likely giving both a large  $\phi$  and  $\theta$  rotation. Now the  $\theta$  rotation is not of great importance as the wider device can simply move the state back to the desired outcome. A sketch of such a setup can be seen in figure 4.1. This architecture will require some changes in the trenching and bonding process, compared to the attempt at making a 2x2 Unitary that was shown in this work.

Another, yet similar, approach is to return to the non-cascaded NOEMS devices. These has a smaller footprint and earlier results show the ability to perform  $\theta > \pi$ . However at this point the possible associated phaseshift due to asymmetries were not analyzed. It would thus be necessary to perform similar measurements on these devices as the ones shown in this report to fully determine this. This would likely be the favorable solution as the overall footprint will decrease by only requiring one of the 2 NOEMS devices to be cascaded. A requirement is however that the initial  $\theta$  rotation can be made without significant  $\phi$  rotation.

## Future work - mechanical modes

Another interesting prospect of the cascaded structures is the more complex mechanical modes arising since the individual parts of the total devices are coupled - possibly leading to coupled modes. For the lowest order modes we primarily observed similar results as for the non-cascaded NOEMS devices, with 2 modes constituting the slightly asymmetrical waveguides. These are primarily the limitation when needing on demand control over photons, as they set a "speed limit" on the operations. A small amount of effort was however put into the study of resonantly driving the system. Here it was found that while driving resonantly with the lowest order mechanical modes was possible, it might be even more interesting to look into the larger order modes, as these can be much faster. We were able

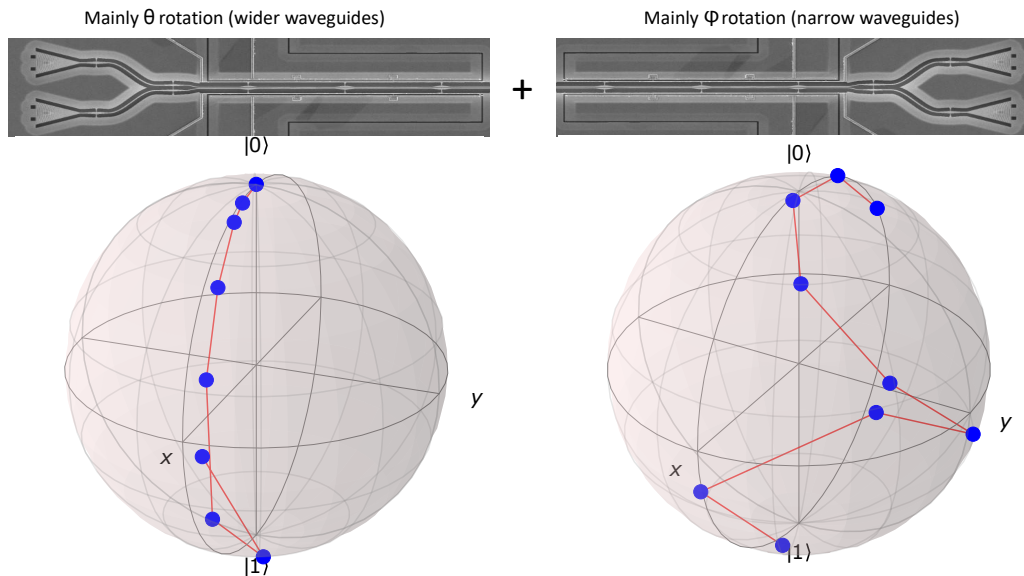


Figure 4.1: **Proposed 2x2 unitary operation with existing structures** a 2x2 unitary that can possibly be achieved with the structures that have been shown in this report. The first NOEMS device primarily constitutes the  $\theta$  rotation with the wider waveguides, here a full  $\pi$ -rotation can be achieved at 6V. Afterwards the asymmetrically based phase shifter with narrower waveguides are added, this can perform a full  $2\pi$ -rotation around  $\phi$  at 8V

to drive with modes allowing for switching times in the order of  $\approx 100$  ns, this might prove to be interesting towards demultiplexing schemes and it is not unlikely that even faster results can be produced.

The analysis of this was not however thorough enough to conclude whether or not this is interesting in and on itself, and some curious results are still to be analyzed. From theory it is clear that resonant driving requires much lower amplitudes, as the response is proportional to the quality factor of the mode in question. However when actuating these modes a comparable large amount of voltage of  $\approx 1V$  was needed to see the effects. Thus further analysis of the properties of these exact modes are necessary in order to fully understand the effects.

One of the challenges towards demultiplexing schemes is that similar resonance frequencies are needed for the different NOEMS devices in the setup. A very interesting feature of the devices for this was however found, it is clear that as there are fabrication limitations and small variations in the geometries of the waveguides, different NOEMS will have varying resonance frequencies. A feature is nevertheless that these can be tuned by applying a DC voltage over the NOEMS due to frequency softening. It was found that at least some of the different devices had resonance frequencies within tuning range of each other. It is thus an interesting future prospect to analyze whether this gives the ability to perform resonant switching of 2 independent devices at the same resonance frequency by simply applying a DC voltage on top of the resonant driving. Importantly however was that not all modes of the systems had these features, it is thus again necessary to have a better understanding of the modes as larger order modes are more interesting towards resonant driving of the system.

# Appendix A

## Phase shift measurements

For the phase shift measurements the following signal was used for the on/off filtering

### A.1 Optimizing tethers

When dealing with the cascaded NOEMS structures we will inevitably need a larger number of tethers in order to keep the system fully suspended. when doing 3 cascaded devices this increases the number of tethers from 1 to 3. The tethering is done by broadening the waveguides from the initial width of  $\approx 200$  nm to a final width of 500 nm. In this region of the structures they will be much less optically active, furthermore the waveguides distances are fixed, meaning that the gap is not changing here, leading to no interaction in this region. The tethers thus constitutes a "dead" region in the device, which only increases the footprint without increasing the optical response.

### A.2 MMI - theory

A method is needed to generate a 50/50 splitting between 2 input ports to be used in the symmetric beamsplitter devices. One method of doing this is by the use of Multi-Mode-

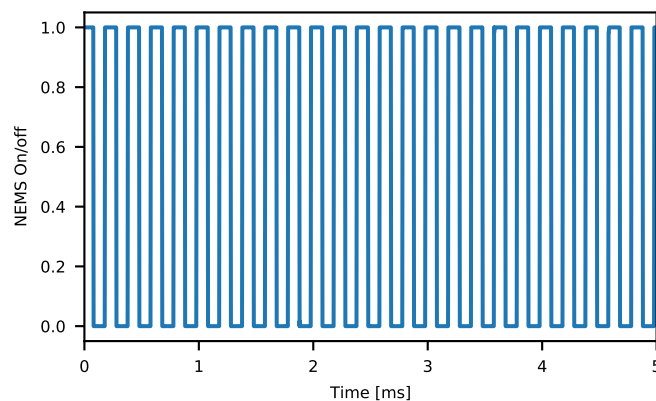


Figure A.1: **NEMS actuation signal** Signal actuating the NEMS system, when it is 0 no voltage is applied, when 1 the voltage is applied. This is applied with a fast Tukey window, which ramps up in  $\approx 1\mu s$ . This ensures that the NEMS system does not start oscillating, as this is slower than the fastest resonant mode. This is used as a mask to filter the signal between the NEMS being actuated and not actuated, such that the response at each individual voltage can be determined.

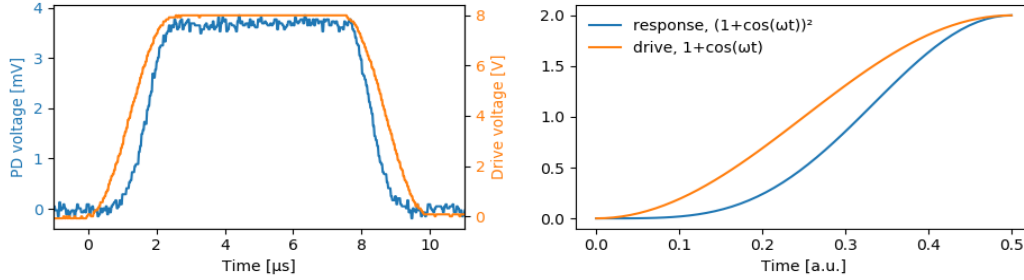


Figure A.2: **Response to a tukey drive** (a) Tukey drive and response (b) zoom in on the response with corresponding curves.

Interferometers. Here a single mode waveguide is tapered into a multimode waveguide. In this case a dual mode waveguide supporting the 2 lowest order TE-modes. The insertion will cause both modes to be excited in the dual mode waveguide. These modes will have different electrical fields and varying effective mode indices. As one mode is symmetric and the other is asymmetric these will interfere with each other. As they have different propagation constants the outcome of the interference will vary. This means that at different points in the waveguide the mode will be located at different positions, this effect is called the beating and is a property of the 2 different effective mode indices. Thus if we are stopping the multimode portion and coupling into 2 single mode waveguides at the correct position, 50% of the light will exit through one of the port while the rest exits the other port. Thus a 50/50 splitting of light through the 2 output ports can be obtained. A limitation to this however is that the beat length is quite short, and is highly dependent on the geometry of the waveguides. Thus small fluctuations in these parameters might greatly influence the exact splitting ratio that is obtained between the ports.

### A.3 Switching speed

Here more effort towards finding switching speeds not inducing oscillations is shown. It is furthermore shown that the optical response of the system does not follow the actuation signal but is rather a bit slower. This happens as the response does not go as  $V$  but rather  $V^2$ .

### A.4 Mechanical modes simulations

Some examples of simulated mechanical modes of the individual parts of a cascaded NOEMS device. Here it is seen that complex modes arise at larger frequencies. From these modes it is difficult to estimate the exact optical effect, but they might prove valuable for resonant driving of the systems.

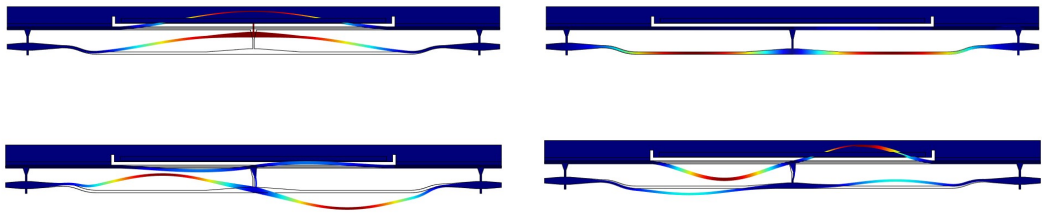


Figure A.3: **Different mechanical modes having different frequencies** The top left shows the lowest order mechanical mode response. Here the waveguides are pulled completely apart, thus this should make for a large change in optical parameters. The top right panel show out of plane movement, which we should not be able to find experimentally

# Bibliography

- [1] R. Uppu, F. T. Pedersen, Y. Wang, C. T. Olesen, C. Papon, X. Zhou, L. Midolo, S. Scholz, A. D. Wieck, A. Ludwig, and P. Lodahl, “Scalable integrated single-photon source,” *Science Advances*, vol. 6, no. 50, p. eabc8268, 2020. (page 2).
- [2] M. Reck, A. Zeilinger, H. J. Bernstein, and P. Bertani, “Experimental realization of any discrete unitary operator,” *Phys. Rev. Lett.*, vol. 73, pp. 58–61, Jul 1994. (pages 2, 3, 18).
- [3] W. R. Clements, P. C. Humphreys, B. J. Metcalf, W. S. Kolthammer, and I. A. Walmsley, “Optimal design for universal multiport interferometers,” *Optica*, vol. 3, pp. 1460–1465, Dec 2016. (page 2).
- [4] P. Kok, W. J. Munro, K. Nemoto, T. C. Ralph, J. P. Dowling, and G. J. Milburn, “Linear optical quantum computing with photonic qubits,” *Reviews of Modern Physics*, vol. 79, pp. 135–174, Jan. 2007. (page 2).
- [5] F. Arute, K. Arya, R. Babbush, D. Bacon, J. Bardin, R. Barends, R. Biswas, S. Boixo, F. Brandao, D. Buell, B. Burkett, Y. Chen, J. Chen, B. Chiaro, R. Collins, W. Courtney, A. Dunsworth, E. Farhi, B. Foxen, A. Fowler, C. M. Gidney, M. Giustina, R. Graff, K. Guerin, S. Habegger, M. Harrigan, M. Hartmann, A. Ho, M. R. Hoffmann, T. Huang, T. Humble, S. Isakov, E. Jeffrey, Z. Jiang, D. Kafri, K. Kechedzhi, J. Kelly, P. Klimov, S. Knysh, A. Korotkov, F. Kostritsa, D. Landhuis, M. Lindmark, E. Lucero, D. Lyakh, S. Mandrà, J. R. McClean, M. McEwen, A. Megrant, X. Mi, K. Michielsen, M. Mohseni, J. Mutus, O. Naaman, M. Neeley, C. Neill, M. Y. Niu, E. Ostby, A. Petukhov, J. Platt, C. Quintana, E. G. Rieffel, P. Roushan, N. Rubin, D. Sank, K. J. Satzinger, V. Smelyanskiy, K. J. Sung, M. Trevithick, A. Vainsencher, B. Villalonga, T. White, Z. J. Yao, P. Yeh, A. Zalcman, H. Neven, and J. Martinis, “Quantum supremacy using a programmable superconducting processor,” *Nature*, vol. 574, p. 505–510, 2019. (page 2).
- [6] A. Crespi, R. Osellame, R. Ramponi, D. J. Brod, E. F. Galvão, N. Spagnolo, C. Vitelli, E. Maiorino, P. Mataloni, and F. Sciarrino, “Integrated multimode interferometers with arbitrary designs for photonic boson sampling,” *Nature Photonics*, vol. 7, pp. 545–549, may 2013. (page 2).
- [7] C. Papon, X. Zhou, H. Thyrrerstrup, Z. Liu, S. Stobbe, R. Schott, A. D. Wieck, A. Ludwig, P. Lodahl, and L. Midolo, “Nanomechanical single-photon routing,” *Optica*, vol. 6, pp. 524–530, Apr 2019. (pages 2, 3, 11, 14, 16, 17, 18, 21, 24, 29, 52).
- [8] J. Carolan, C. Harrold, C. Sparrow, E. Martín-López, N. J. Russell, J. W. Silverstone, P. J. Shadbolt, N. Matsuda, M. Oguma, M. Itoh, G. D. Marshall, M. G. Thompson, J. C. F. Matthews, T. Hashimoto, J. L. O’Brien, and A. Laing, “Universal linear optics,” *Science*, vol. 349, no. 6249, pp. 711–716, 2015. (pages 2, 5).

- [9] N. C. Harris, Y. Ma, J. Mower, T. Baehr-Jones, D. Englund, M. Hochberg, and C. Galland, “Efficient, compact and low loss thermo-optic phase shifter in silicon,” *Opt. Express*, vol. 22, pp. 10487–10493, May 2014. (pages 2, 54).
- [10] R. Warburton, “Single spins in self-assembled quantum dots,” *Nature materials*, vol. 12, pp. 483–93, 06 2013. (page 2).
- [11] T. Rudolph, “Why i am optimistic about the silicon-photonics route to quantum computing,” *APL PHOTONICS*, vol. 2, 2017. (page 2).
- [12] P. Lodahl, S. Mahmoodian, and S. Stobbe, “Interfacing single photons and single quantum dots with photonic nanostructures,” *Reviews of Modern Physics*, vol. 87, pp. 347–400, may 2015. (pages 2, 3).
- [13] Z. Lu, H. Yun, Y. Wang, Z. Chen, F. Zhang, N. A. F. Jaeger, and L. Chrostowski, “Broadband silicon photonic directional coupler using asymmetric-waveguide based phase control,” *Opt. Express*, vol. 23, pp. 3795–3808, Feb 2015. (page 3).
- [14] P. Wittek, “4 - quantum computing,” in *Quantum Machine Learning* (P. Wittek, ed.), pp. 41–53, Boston: Academic Press, 2014. (page 3).
- [15] F. Lenzini, B. Haylock, J. C. Lored, R. A. Abranches, N. A. Zakaria, S. Kasture, I. Sagnes, A. Lemaitre, H.-P. Phan, D. V. Dao, P. Senellart, M. P. Almeida, A. G. White, and M. Lobino, “Active demultiplexing of single photons from a solid-state source,” *Laser & Photonics Reviews*, vol. 11, no. 3, p. 1600297, 2017. (pages 4, 18).
- [16] H. Kogelnik, *2. Theory of dielectric waveguides*, pp. 13–81. Berlin, Heidelberg: Springer Berlin Heidelberg, 1975. (page 7).
- [17] E. Rosencher and B. Vinter, *Optoelectronics*. Cambridge University Press, 2002. (page 7).
- [18] X. Zhou, I. V. Kulkova, T. Lund-Hansen, S. L. Hansen, P. Lodahl, and L. Midolo, “High-efficiency shallow-etched grating on gaas membranes for quantum photonic applications,” *Applied Physics Letters*, 2018. (page 8).
- [19] P. Lodahl, “Quantum-dot based photonic quantum networks,” 2017. (page 8).
- [20] T. Tsuchizawa, K. Yamada, H. Fukuda, T. Watanabe, J. ichi Takahashi, M. Takahashi, T. Shoji, E. Tamechika, S. Itabashi, and H. Morita, “Microphotonic devices based on silicon microfabrication technology,” *IEEE Journal of Selected Topics in Quantum Electronics*, vol. 11, no. 1, pp. 232–240, 2005. (pages 8, 29).
- [21] A. Szameit, F. Dreisow, T. Pertsch, S. Nolte, and A. Tünnermann, “Control of directional evanescent coupling in fs laser written waveguides,” *Opt. Express*, vol. 15, pp. 1579–1587, Feb 2007. (page 8).
- [22] W.-P. Huang, “Coupled-mode theory for optical waveguides: an overview,” *J. Opt. Soc. Am. A*, vol. 11, pp. 963–983, Mar 1994. (page 9).
- [23] W. S. C. Chang, *Fundamentals of Guided-Wave Optoelectronic Devices*. Cambridge University Press, 2009. (page 10).
- [24] S. Fugger, *Design and characterization of nano-mechanical quantum photonic devices*. PhD thesis, 2021. (pages 11, 24).

- [25] J. Yan, A. A. Seshia, K. L. Phan, P. G. Steeneken, and J. T. van Beek, "Narrow bandwidth single-resonator mems tuning fork filter," in *2007 IEEE International Frequency Control Symposium Joint with the 21st European Frequency and Time Forum*, pp. 1366–1369, 2007. (page 18).
- [26] M. Saygin, I. Kondratyev, I. Dyakonov, S. Mironov, S. Straupe, and S. Kulik, "Robust architecture for programmable universal unitaries," *Physical Review Letters*, vol. 124, jan 2020. (page 18).
- [27] *Microsystem Design*. Springer (India) Pvt. Limited, 2006. (pages 19, 28).
- [28] S. L. Miller and D. Childers, "10 - power spectral density," 2004. (pages 22, 27).
- [29] S. Jesse, S. V. Kalinin, R. Proksch, A. P. Baddorf, and B. J. Rodriguez, "The band excitation method in scanning probe microscopy for rapid mapping of energy dissipation on the nanoscale," *Nanotechnology*, vol. 18, p. 435503, sep 2007. (page 22).
- [30] S. Rahimi-Keshari, M. A. Broome, R. Fickler, A. Fedrizzi, T. C. Ralph, and A. G. White, "Direct characterization of linear-optical networks," *Opt. Express*, vol. 21, pp. 13450–13458, Jun 2013. (page 26).
- [31] M. Sucher, J. Fox, and M. Wind, *Handbook of Microwave Measurements*. No. vb. 3 in Handbook of Microwave Measurements, Polytechnic Press of the Polytechnic Institute of Brooklyn, 1963. (page 28).
- [32] M. A. Nielsen and I. L. Chuang, *Quantum Computation and Quantum Information: 10th Anniversary Edition*. USA: Cambridge University Press, 10th ed., 2011. (page 38).